AD-A259 743

INTATION PAGE

Form Approved
OMB No. 0704-0188

2. REPORT DATE	3. REPORT TYPE AND DATES COVERED
	ANNUAL 01 Oct 91 TO 30 Sep 92

4. TITLE AND SUBTITLE
SOURCE MECHANISMS AND RADIO EFFECTS OF IONOSPHERIC PLASMA

5. FUNDING NUMBERS
F49620-92-J-0001
61102F
2310
BS

6. AUTHOR(S)
DR MIN-CHANG LEE

7. PERFORMING ORGANIZATION NAME(S) AND ADDRESS(ES)
Boston University
Boston, MA 02215

8. PERFORMING ORGANIZATION REPORT NUMBER
AFOSR-TR- 93 1007

9. SPONSORING/MONITORING AGENCY NAME(S) AND ADDRESS(ES)
Lt Col Stobie
AFOSR/NL
Building 410
Bolling AFB DC 20332-6448

10. SPONSORING/MONITORING AGENCY REPORT NUMBER
93-01485

11. SUPPLEMENTARY NOTES

12a. DISTRIBUTION/AVAILABILITY STATEMENT
Approved for public release;
distribution unlimited

12b. DISTRIBUTION CODE

13. ABSTRACT *(Maximum 200 words)*

Since October 1, 1991 experimental and theoretical research has been conducted by Prof. Min-Chang Lee and his students at BU and MIT. This research work is aimed at investigating the ionospheric plasma disturbances which can affect significantly the radio wave propagation in communications and space surveillance. The research topics which have been investigated include: (1) A source mechanism leading to the symmetric lower hybrid sidebands and a low-frequency mode in the upper atmosphere, (2) Characteristics of lightning-induced plasmas, (3) Radio wave-produced plasmas and effects on radio communications, (4) Plasma turbulence and formation of field-aligned density fluctuations as ionospheric ducts.

14. SUBJECT TERMS	15. NUMBER OF PAGES
	16. PRICE CODE

17. SECURITY CLASSIFICATION OF REPORT	18. SECURITY CLASSIFICATION OF THIS PAGE	19. SECURITY CLASSIFICATION OF ABSTRACT	20. LIMITATION OF ABSTRACT
(U)	(U)	(U)	(UL)

NSN 7540-01-280-5500

Standard Form 298 (Rev. 2-89)
Prescribed by ANSI Std. Z39-18

93 1 26 103

Annual Report
F49620-92-J-0001

Plasma Fusion Center
Massachusetts Institute of Technology
Cambridge, Massachusetts 02139
Telephone: 617/253-8100

To: Lt. Col. James G. Stobie, Program Manager, AFOSR

From: Prof. Min-Chang Lee MCL

Date: November 1, 1992

Re: Progress Report on Sponsored Research Programs titled "Source Mechanism and Radio Effects of Ionospheric Plasma Disturbances" (F49620-92-J-0001) and "Studies of Enhanced Radar Backscatter" ~~(F49620-92-J-0297)~~

Since October 1, 1991 experimental and theoretical research has been conducted by Prof. Min-Chang Lee and his students at BU and MIT under the sponsorship of Lt. Col. James G. Stobie's office at AFOSR (grant # AFOSR-92-0001 and F49620-92-J-0297). This research work is aimed at investigating the ionospheric plasma disturbances which can affect significantly the radio wave propagation in communications and space surveillance. The research topics which have been investigated include: (1) A source mechanism leading to the symmetric lower hybrid sidebands and a low-frequency mode in the upper atmosphere, (2) Characteristics of lightning-induced plasmas, (3) Radio wave-produced plasmas and effects on radio communications, (4) Plasma turbulence and formation of field-aligned density fluctuations as ionospheric ducts. Progress in these research subjects are briefly described below.

(1) A low-frequency ($\sim 500Hz$) mode in conjunction with symmetric sidebands, displayed by approximately 500 Hz off the carrier frequencies of 11.90 and 12.65 kHz, has been observed in experiments conducted with the Aureol 3 satellite at altitudes of 1200 km above the Komsomolsk-on-Amur Alpha Station (50^0N, 135^0E) (Sotnikov et al., 1991 and references therein). These observations are examined and interpreted with an alternative mechanism based on the theory of Lee and Kuo [1984]. The proposed mechanism suggests that the injected VLF wave parametrically excites a purely growing mode and both the Stokes and anti-Stokes sidebands of the lower hybrid waves. The Doppler-shifted frequencies of these modes resulting from the satellite motion adequately account for both the sidebands and the low-frequency mode observed in the Aureol 3 experiments. This

work will be published in an JGR paper (1992) by Dalkir, Lee, Groves, and Kuo.

(2) The scattering of radio waves from lightning-induced plasmas is investigated. the plasmas are modeled as long, thin, perfectly conducting vertical channels with surface density irregularities on a scale much smaller than the total channel length. the theoretically predicted wavelength dependence of the radar reflectivity is compared to experimental results obtained with the MIT C-band, S-band, and the Millstone-Hill UHF radars. It is found that the rough surface scattering model can adequately account for the $1/\lambda^2$ wavelength dependence of the radar reflectivity observed in the MIT-Millstone Hill experiments, if the density fluctuations of the lightning-induced plasmas have a power-law type spectrum. The results of this work has been reported in a paper submitted recently to JGR for publication by Dalkir, Lee, and Williams.

(3) The scattering of radio waves from perfectly conducting, rough plasma surfaces is investigated. Cylindrical plasma channnel created by lightning discharges and disk-shaped plasmas generated by a single radio beam are examined. The surface density irregularities of the plasmas are modelled as random perturbations of the constant density background, characterized by either a Gaussian or power-law type spectrum. The theoretical wavelength dependence of the radar reflectivity of the lightning plasmas is compared to experimental results obtained with the MIT C-band, S-band, and the Millstone UHF radars. The rough surface scattering model can adequately account for the $1/\lambda^2$ wavelength dependence of the radar reflectivity observed in the MIT-Millstone Hill experiments, if the surface density irregularities have a power-law type spectrum. The efficiency of reflection of radio waves from an artificially generated plasma in both monostatic and bistatic radar geometries is discussed. In radio communication and space surveillance applications, the surface density irregularities may significantly affect the reflectivity of the artificial plasma patch, depending on the power spectrum of the plasma density irregularities. The results of the work are presented in a paper submitted to the technical journal titled "Radio Science"for publication by Dalkir and Lee.

(4) In our recent ionospheric heating experiments at Arecibo, Puerto Rico, we investigated the spectral characteristics of HF enhanced Langmuir waves among other phenomena. The obliquely propagating HF waves were transmitted from a tilted heater in experiments during August 5 - 11, 1992, while the vertically propagating HF waves were employed in experiments during September 17 - 22, 1992. In the "oblique heating" experiments, the main beam of the HF heater waves was tilted by 12^0 to the north, while the first sidelobe pointed 13^0 to the south. The radiated power of the first side-

lobe was estimated to be only slightly different ($\sim 1dB$) from that of the main beam (D.B. Muldrew, personal communication, 1992). Thus, the illuminated ionospheric region was presumably much greater than that with the vertically transmitted waves from the heater. The cascading spectra of the PDI (parametric decay instabilities) produced Langmuir waves were observed in the vertical heating experiments as expected. The radar measurements of the HF enhanced plasma lines in the oblique heating experiments also showed the excitation of PDI; however, the cascading spectrum was not seen. Rather, a broad, highly structured spectrum separated from the PDI produced spectrum by 15 kHz or so with higher power was generated. It indicates that other process(es) excited by the obliquely propagating heater waves can compete with the PDI. Our comparative studies of Langmuir waves produced by the vertically and obliquely transmitted HF heater are aimed at invesitigating the source mechanisms responsible for the generation of HF enhaced Langmuir waves. Parametric instabilities and nonlinear scattering processes will be examined as the potential mechanisms. This work will be presented by Lee, Sanchez, Kuo, Moriarty, Sulzer, and Groves at the National Radio Science Meeting of URSI to be held in Boulder, Colorado during January 6-9, 1993.

These research projects lead to the publications and presentation of the following papers and students' theses:

(A) Publications in Refereed Journals:

(1) Y.R. Dalkir, M.C. Lee, K.M. Groves, and S.P. Kuo, "A mechanism responsible for the observation of symmetric lower hybrid sidebands and a low frequency mode in the upper ionosphere", accepted for publication in the Journal of Geophysical Research, 1992.

(2) Y.R. Dalkir, M.C. Lee, E.R. Williams, "Radio reflectivity of lightning induced plasmas", submitted to the Journal of Geophysical Research for publicationh, 1992.

(3) Y.R. Dalkir, and M.C. Lee, "Radar studies of lightning induced plasmas with potential applications to radio communications and space surveillance", submitted to Radio Science for publication, 1992.

(B) Graduate Students' Theses:

K.D. Vilece, "Experimental study of anti-Stokes Langmuir modes and particle precipitation produced by RF heating of ionospheric plasmas", Master Thesis, Department

of Nuclear Engineering, MIT, 1992.

L.A. Sanchez, "Studies of artificial spread F phenomenon with tilted HF heater at Arecibo, Puerto Rico", Master Thesis, Department of Electrical, Computer, and Systems Engineering, Boston University, in progress, 1992.

(C) Presentations in Conferences:

(1) "Nonlinear interactions of VLF waves with ionospheric plasmas", by M.C. Lee, K.M. Groves, Y.R. Dalkir, and S.P. Kuo, presented at the URSI- National Radio Science Meeting, University of Colorado, Boulder, Colorado, January 7-10, 1992.

(2) "Anti-Stokes Langmuir modes produced by high power HF waves at Arecibo, Puerto Rico", by M.C. Lee, K.D. Vilece, K.M. Groves, and S.P. Kuo, presented at the URSI-National Radio Science Meeting, University of Colorado, Boulder, Colorado, January 7-10, 1992.

(3) "Frequency-upshifted Langmuir modes produced by RF heating of ionospheric plasmas", by M.C. Lee, K.D. Vilece, Y.R. Dalkir, K.M. Groves, and S.P. Kuo, presented at the 1992 IEEE International Conference on Plasma Science, Tampa, Florida, June 1-3, 1992.

(4) "Experimental studies of nonlinear wave propagation and interactions with magnetized plasmas", by M.C. Lee, D.T. Moriarty, M. Onozuka, K.D. Vilece, R.R. Parker, and S.P. Kuo, presented at the 1992 IEEE International Conference on Plasma Science, Tampa, Florida, June 1-3, 1992.

(5) "Satellite measurements of symmetric lower hybrid sidebands and a low frequency mode during VLF wave injection", Y.R. Dalkir, M.C. Lee, K.M. Groves, and S.P. Kuo, presented at the 1992 International Beacon Satellite Symposium, Massachusetts Institute of Technology, Cambridge, Massachusetts, July 6-10, 1992.

(6) "Generation of artificial ionospheric ducts for guided VLF wave propagation", by M.C. Lee, S. Basu, K.M Groves, K.L Koh, R. Singh, M.P. Sulzer, and K.D. Vilece, presented at the 1992 International Beacon Satellite Symposium, Massachusetts Institute of Technology, Cambrdige, Massachusetts, July 6-10, 1992.

(7) "Laboratory simulation of anomalous absorption of radio waves in turbulent magnetoplasmas", by D.T. Moriarty, M.C. Lee, M. Onozuka, R.R. Parker, and K.D. Vilece,

presented at the 1992 International Beacon Satellite Symposium, Massachusetts Institute of Technology, Cambrdige, Massachusetts, July 6-10, 1992.

(8) "Analysis of wave scattering off a two dimensional plasma density irregularities in the ionosphere", by A.Y. Ho, S.P. Kuo, and M.C. Lee, presented at the 1992 International Beacon Satellite Symposium, Massachusetts Institute of Technology, Cambrdige, Massachusetts, July 6-10, 1992.

(9) "Scintillation effects on incoherent scatter radar observations of enhanced ion acoustic waves", by K.M. Groves, M.C. Lee, J.C. Foster, and F.T. Djuth, presented at the 1992 International Beacon Satellite Symposium, Massachusetts Institute of Technology, Cambrdige, Massachusetts, July 6-10, 1992.

A Mechanism Responsible for the Observation of Symmetric Lower Hybrid Sidebands and a Low Frequency Mode in the Upper Ionosphere

Y. R. DALKIR AND M. C. LEE

Plasma Fusion Center, Massachusetts Institute of Technology, Cambridge, Massachusetts

K. M. GROVES

Ionospheric Physics Division, Phillips Laboratory, Hanscom Air Force Base, Massachusetts

S. P. KUO

Weber Research Institute, Polytechnic University, Farmingdale, New York

A low-frequency (~500 Hz) mode in conjunction with symmetric sidebands, displaced by approximately 500 Hz off the carrier frequencies of 11.90 and 12.65 kHz, has been observed in experiments conducted with the Aureol 3 satellite at altitudes of 1200 km above the Komsomolsk-on-Amur Alpha Station (50°N, 135°E) (*Sotnikov et al.*, 1991 and references therein). These observations are examined and interpreted with an alternative mechanism based on the theory of *Lee and Kuo* [1984]. The proposed mechanism suggests that the injected VLF wave parametrically excites a purely growing mode and both the Stokes and anti-Stokes sidebands of the lower hybrid waves. The Doppler- shifted frequencies of these modes resulting from the satellite motion adequately account for both the sidebands and the low-frequency mode observed in the Aureol 3 experiments.

1. INTRODUCTION

Symmetric electrostatic sidebands displaced by approximately 500 Hz above and below the carrier VLF frequency have been observed by *Tanaka et al.*, [1987, and references therein] and others in experiments conducted at the Komsomolsk-on-Amur Alpha station (50°N, 135°E). The sidebands were recorded by the Aureol 3 satellite at L - values between 1.7 and 2.0, at an altitude of 1200 km above the transmitter, which was operated at 11.90 and 12.65 KHz. The sidebands were observed only in conjunction with a low-frequency mode, located at approximately 500 Hz. In an interesting follow-up paper, *Sotnikov et al.* [1991] suggest the low-frequency mode is naturally-occurring ELF hiss similar to that observed on other low-altitude satellites [*Gurnett and Burns*, 1968; *Mosier*, 1971; *Muzzio and Angerami*, 1972] which couples nonlinearly carrier wave to produce the observed sidebands.

The purpose of this paper is to discuss a different mechanism which can also account for the prominent features of the sidebands and the low- frequency modes reported by *Tanaka et al.*, [1987, and references therein]. In this proposed mechanism, based on the theory of *Lee and Kuo* [1984], the low-frequency mode is not a naturally occurring electromagnetic (em) emission, but is a field-aligned purely growing mode excited parametrically by the injected VLF wave. The symmetric sidebands are the Stokes and anti-Stokes components of the excited lower hybrid waves (LHW). The theory shows that the frequency shifts of the sidebands are comparable in magnitude to the observed fre-

quency of the low frequency mode, which is in good agreement with the results reported by *Sotnikov et al.* [1991] and *Tanaka et al.* [1987].

The essential difference between the mechanism proposed in this paper and that outlined by *Sotnikov et al.* [1991] is the interpretation of the low-frequency mode: *Sotnikov et al.* [1991] suggest that it is a real frequency, small wave number mode; by contrast, we propose that it has a large wave number, and that the observed frequency is a Doppler effect arising from the satellite motion. The electric and magnetic fields of the emissions were measured by means of spheres located on insulated booms on the Aureol 3 spacecraft; this equipment cannot differentiate a real frequency from a Doppler shift effect. Thus the possibility of a field-aligned purely growing density striation giving rise to the observed low-frequency mode cannot be ruled out [*Sotnikov et al.*, 1991]. Our proposed mechanism explains not only the generation of the LHW sidebands but predicts the concomitant occurrence of this low-frequency mode.

Section 2 describes the highlights of the theory, and its applicability to *Tanaka et al.'s* [1987] observations. The frequency shift of the sidebands, the threshold incident electric field for the mechanism, and the growth rate of the instability are estimated in this section. Section 3 discusses some further characteristics of the low-frequency mode, including its electrostatic or electromagnetic character and its wave vector angle, that are relevant to the analysis. Conclusions follow in section 4.

2. Proposed Mechanism

Lee and Kuo [1984] propose that symmetric lower hybrid sidebands can be parametrically generated by an intense VLF wave in the ionosphere and magnetosphere. In addition, a field-aligned purely growing mode with a wave vector comparable in magnitude to those of the sidebands is excited concomitantly at the expense of the VLF pump wave. The frequencies of these waves as observed by the satellite arise from the Doppler shift: $f = \mathbf{k} \cdot \mathbf{V}_s/2\pi$ where V_s, the satellite velocity, is approximately 8 km/s, and $\mathbf{k}$ represents the wave vectors of the excited wave modes.

VLF waves injected into the ionosphere from a ground station change to circularly polarized ducted whistler waves with wave vector $\mathbf{k}_0 = k_0\mathbf{e}_z$ and electric field $\mathbf{E} = (\hat{\mathbf{x}} + i\hat{\mathbf{y}})\, E_0 \exp[i(k_0 z - \omega_0 t)]$, where ω_0 is the wave frequency, and the z axis of a Cartesian coordinate system has been taken along the geomagnetic field. This pump wave may then excite the Stokes and anti-Stokes sidebands of lower hybrid waves [(k_-, ω_-) and (k_+, ω_+), respectively] together with a purely growing or zero-frequency mode $(\mathbf{k}_s, \omega_s)$ according to the following wave vector and frequency matching relations:

$$\omega_+ - \omega_s = \omega_0 = \omega_- + \omega_s^* \qquad (1)$$

$$\mathbf{k}_+ - \mathbf{e}_x k_s = \mathbf{e}_z k_0 = \mathbf{k}_- + \mathbf{e}_x k_s \qquad (2)$$

Under the assumption that the low-frequency mode is purely growing ($\omega_s = i\gamma$) and that its wave vector is perpendicular to the geomagnetic field ($\mathbf{k}_s = k_s \mathbf{e}_x$), equations (1) and (2) reduce to

$$\omega_\pm = \omega_0 + i\gamma$$

$$\mathbf{k}_\pm = \mathbf{e}_z k_0 \pm \mathbf{e}_x k_s$$

Furthermore, $k_s >> k_0$, and thus $k_\pm \sim k_s$.

The magnitude of the wave number of the sidebands can be calculated by substituting the parameters relevant for the Aureol 3 experiments as provided by *Sotnikov et al.* [1991] into the lower hybrid wave dispersion relation:

$$\mathrm{Re}(\omega_\pm) = \omega_0 \sim \omega_{pi}(1 + \frac{\omega_{pe}^2}{\Omega_e^2})^{-1/2}(1 + \frac{M k_0^2}{m k_s^2})^{1/2}$$

where ω_{pe}/Ω_e is the ratio of the electron plasma frequency to the electron gyrofrequency. At 1200 km, $\Omega_e = 2\pi \cdot 850$ kHz for $B_0 = 3 \cdot 10^{-5}$ T, and m/M is the ratio of the electron mass to the ion mass. The magnitude of the wave vector k_0 is obtained from the ducted whistler wave dispersion relation $k_0 = (\omega_{pe}/c)(\omega_0/\Omega_e)^{1/2}$. The resulting maximum Doppler shifted frequency of the sidebands is given approximately by $(\omega_0 \pm |k_s V_s|)/2\pi$, where $\omega_0/2\pi$ is the carrier frequency. The Doppler shifted frequency is reduced from this value when the satellite moves across the Earth's magnetic field at an angle that is not exactly 90°.

Figure 1 displays the results of calculations of the maximum sideband frequency displacement over a range of ion concentration ($\omega_{pe}/\Omega_e = 0.5 - 0.85$) for the two carrier frequencies, 11.90 kHz and 12.65 kHz. For an ion composition that is predominantly H^+, the graph shows that large-frequency displacements are possible near those ion concentrations where the carrier frequency approaches the lower hybrid resonance frequency. This occurs at approximately $\omega_{pe}/\Omega_e = 0.74$ and 0.83 for $\omega_0/2\pi = 11.90$ and 12.65 kHz respectively. A 500-Hz sideband frequency displacement is expected in the range $\omega_{pe}/\Omega_e = 0.73 - 0.80$. By contrast, if O^+ is the dominant species, only small frequency shifts ($\leq$ 100 Hz) are possible. The actual ion composition of the relevant region of the ionosphere can be estimated from data compiled from experiments performed with the Explorer 31 satellite [*Hoffman and Dodson*, 1980]. The altitude of 1200 km at an L -value of 2.0 is actually within the transition region between O^+ to H^+ as the dominant ion species. Where H^+ predominates, the daytime ion concentration lies in the range $\omega_{pe}/\Omega_e = 0.70 - 0.80$. Referring again to Figure 1, it can be seen that this is the range in which a 500-Hz sideband displacement is possible.

Furthermore, the requirement that $\mathbf{k}_\pm \approx \mathbf{k}_s$ implies that the purely growing mode should be observed at a Doppler frequency of $f_s = \mathbf{k}_s \cdot \mathbf{V}_s/2\pi \approx \mathbf{k}_\pm \cdot \mathbf{V}_s/2\pi$ which is approximately equal to the frequency shift of the sidebands. Figure 2 of *Sotnikov et al.* [1991] indicates that the maximum oc-

Fig 1

currence of the lower sidebands is at 500 to 600 Hz below the transmitter frequency, the maximum occurrence of the upper sidebands is 500 to 650 Hz above the transmitter frequency, and the maximum occurrence of the low frequency modes is between 500 and 600 Hz. Thus the data are in good agreement with the predictions of *Lee and Kuo* [1984] as illustrated in Figure 1.

Sidebands will be generated only if the injected VLF wave is intense enough; *Lee and Kuo*'s mechanism requires an incident electric field threshold of [*Lee and Kuo*, 1984, equations (21) and (22)]

domain 1: $\omega_{LH}[1+(M/m)(v_{te}^2/c^2)(\omega_{pe}^2/\Omega_e^2)]^{1/2} < \omega_0 < \omega_{pi}$

$$E_m = 1.2\frac{m}{e}\nu_e v_{te}|\eta|^{1/2}\ (\mathrm{V/m})$$

domain 2: $\omega_{pi} < \omega_0$

$$E_m = 0.86(k_s^2 v_{te}^3/\Omega_e)(m/e)(1+(1+4\Omega_e^2\nu_e^2\eta^2 /k_s^4\nu_{te}^4)^{1/2})^{1/2}/|\eta|^{1/2}\ (\mathrm{V/m})$$

where ω_{LH} is the lower hybrid resonance frequency, ω_{pi} is the ion plasma frequency, ν_e is the effective electron collision frequency, v_{te} is the electron thermal velocity and where $\eta = [1+(M/m)(k_0/k_s)^2]/[1-(M/m)(k_0/k_s)^2(\Omega_e/\omega_{pe})^2]$. Parameters for the upper ionosphere have been estimated as follows: $v_{te} = (k_B T/m)^{1/2} \sim 1.3\cdot 10^5$ m/s for $T_e \sim 1000$K; $\nu_e = \left(59 + 4.18\log(\frac{T_e^3}{n_0})\right)10^{-6}T_e^{-3/2}n_0 \sim 10$ Hz; where n_0 has been calculated from the electron plasma frequency: $n_0 = \omega_{pe}^2\epsilon_0 m/e^2$. The relevant regime for an H^+ plasma is domain 1, with resulting threshold electric fields of $E_m = 8\ \mu$V/m for $\omega_0/2\pi = 11.90$ kHz and between 9 and 10 μV/m for $\omega_0/2\pi = 12.65$ kHz over the range $\omega_{pe}/\Omega_e = 0.7-0.8$. A plasma whose primary ion composition is O^+ falls in domain 2, with $E_m = 15-20\ \mu$V/m for $\omega_{pe}/\Omega_e = 0.7-0.8$ and $\omega_0/2\pi = 11.90$ and 12.65 kHz. The Komsomolsk-on-Amur alpha transmitter was operated at a power of 500 kW [*Tanaka et al.*, 1987] which can produce an incident electric field of at least a few millivolts per meter at an altitude of 1200 km [*Sotnikov et al.*, 1991]; this clearly exceeds the required threshold for the sideband excitation by 2 to 3 orders of magnitude. Thus the VLF pump waves are indeed intense enough to excite the instability in the upper ionosphere.

Lastly, one can estimate the optimum growth rate of the instability, given by [*Lee and Kuo*, 1984, equation (20b)]

$$\gamma \sim 1.4(\nu_e k_s^2 v_{te}^2/\Omega_e^2)E_0/E_m\ (\mathrm{s}^{-1})$$

where E_0 taken to be 10 mV/m is the incident electric field of the pump wave. For an H^+ plasma giving rise to a 500-Hz shift, $\gamma \sim 2\ \mathrm{s}^{-1}$; by contrast, for an O^+ plasma producing a 100-Hz sideband displacement, $\gamma \sim 0.03\ \mathrm{s}^{-1}$. In the Aureol 3 experiments, the alpha transmitter pulse duration was 0.4 s [*Tanaka et al.*, 1987], which is sufficient for the 500-Hz, H^+-induced sidebands to be excited, but is too short for the 100-Hz , O^+ modes to be induced.

3. Discussion

The calculations presented in section 2 show that the theory of *Lee and Kuo* [1984] can successfully account for the 500-Hz frequency shift of the symmetric sidebands, as well the concurrent low-frequency mode observed at 500 Hz by *Tanaka et al.* [1987]. This section considers a few additional aspects of the data that further test the applicability of the proposed mechanism, i.e. the magnetic characteristics of the low-frequency mode, the angle of its wave vector to the geomagnetic field, power plots of the phenomenon, and the ion concentration of the relevant region of the ionosphere.

Sotnikov et al. [1991] suggest that the low frequency modes at 500 Hz are clearly electromagnetic (namely, ELF waves), whereas the symmetric sidebands are electrostatic. The data plots of the magnetic field and electric field intensity versus frequency presented in Figure 1 of their paper, however, do not seem to support this suggestion. (We, however, note that other data sets shown in *Tanaka et al.* [1987] do support the suggestion of *Sotnikov et al.* [1991].) In the original analysis of the data by *Tanaka et al.* [1987], the minimum electric (E) and magnetic (B) field intensities recorded by their equipment are assumed to correspond to electromagnetic emissions. The index of refraction calculated from these minimum levels is found to be $cB/E = 23$. An index of refraction much smaller than this reference value (e.g. $cB/E = 7$) implies that the corresponding mode is quasi-electrostatic. The ELF data analyzed by Sotnikov et al. yielded a value of cB/E statistically on the order of 60 (Y. Tanaka, personal communication, 1992). The data presented in Figure 1 of *Sotnikov et al.* [1991], however, have an index of refraction of approximately 6 at 500 Hz, which indicates that that this is an electrostatic mode. Thus low-frequency modes at 500 Hz or so of both an electrostatic (ES) and electromagnetic (EM) nature have been observed in the Aureol 3 experiments. Furthermore, ELF hiss phenomena in this frequency range have been observed to be intensified at latitudes above VLF transmitters, indicating these modes may not be entirely naturally occurring, but likely to be generated by the VLF waves injected into the ionosphere at these latitudes [*Parrot*, 1990].

A further requirement of the proposed mechanism is that the density striations produced by the low-frequency mode be field aligned, i.e., the wave vector ($\mathbf{k}_s$) should be perpendicular to the geomagnetic field. *Sotnikov et al.* [1991] estimate the wave vector angle to be $\theta_2 \geq 65°$. In addition, *Tanaka et al.* [1987] state that there is no direct evidence to rule out electrostatic characteristics of the ELF emissions, such as proton cyclotron waves propagating almost perpendicularly to the geomagnetic field. Thus the requirement of a right angle between the low frequency wave vector and the geomagnetic field is consistent with the observations.

Data plots of the relative power of the transmitter, the ELF emission/low frequency mode and the sidebands for the Aureol 3 data are presented in Figure 6 of *Lagoutte et al.* [1989]. The authors show convincingly that the power of the

sidebands increases simultaneously with the low frequency mode, while the received power of the transmitted VLF wave is decreased. This is consistent with the proposed instability process, which generates both the sidebands and the purely growing mode at the expense of the incident pump wave.

Lastly, the mechanism proposed in section 2 requires an ion concentration of H^+ in the relevant region of the ionosphere to produce a 500-Hz frequency shift. The mechanism cannot operate if O^+ is the dominant species, since the growth time of the instability in this case is approximately two orders of magnitude larger than the incident pulse duration. The altitude of 1200 km at an L -value of 2 is actually within the transition region of the ionosphere from O^+ to H^+ as the dominant ion species [Hoffman and Dodson, 1980]. Which species is actually more abundant at the altitude of the satellite depends on various factors, such as the time of day and the solar cycle [*Hoffman and Dodson*, 1980]. The proposed mechanism can only generate the observed sidebands and low-frequency mode when H^+ is dominant; this may explain why the sidebands were observed only occasionally by *Tanaka et al.* [1987].

4. Conclusion

The proposed mechanism, based on the theory of *Lee and Kuo* [1984], successfully explains the occurrence of symmetric electrostatic sidebands together with a low-frequency mode generated by VLF waves propagating through the upper ionosphere [*Sotnikov et al.*, 1991, and references therein]. The parametric excitation mechanism, whereby both the Stokes and anti-Stokes components of lower hybrid waves are generated together with a purely growing mode, in a plasma where H^+ is dominant, can account for the magnitude of the frequency shift of the sidebands and predict the occurrence of the low frequency mode. The magnetic properties of this ELF mode, its possible large wave vector angle with respect to the geomagnetic field, studies of the relative power intensities of the generated modes and the transmitted wave, and the ion concentration in the region are all consistent with the proposed mechanism. Thus we conclude that a Doppler shift effect, in contrast to the real frequency modes proposed by *Sotnikov et al.* [1991], can also be a plausible mechanism responsible for both the sideband structures and the low frequency modes observed in the Aureol 3 experiments.

Acknowledgments. This work has been supported by AFOSR grants F49620-92-J-0103 and AFOSR-92-0001 and NSF grant ATM-9016235 at the Massachusetts Institute of Technology and by NSF grant ATM-9024827 at the Polytechnic University.

The Editor thanks Y. Tanaka and another referee for their assistance in evaluating this paper.

References

Gurnett, D. A., and T. B. Burns, The low frequency of ELF emissions, *J. Geophys. Res.*, *73*, 7437, 1968.

Hoffman, J.H., and W.H. Dodson, Light ion concentrations and fluxes in the polar regions during magnetically quiet times, *J. Geophys. Res., 85,* 626, 1980.

Lagoutte, D., F. Lefeuvre, and J. Hanasz, Application of bicoherence analysis in study of wave interactions in space plasma, *J. Geophys. Res., 94,* 435, 1989.

Lee, M.C. and S.P. Kuo. Production of lower hybrid waves and field-aligned plama density striations by whistlers, *J. Geophys. Res., 89,* 10,873, 1984.

Mosier, S. R., Poynting flux studies of hiss with the INJUN 5 satellite, *J. Geophys. Res., 76,* 1713, 1971.

Muzzio, J.L.R., and J.J. Angerami, OGO 4 observations of extremely low-frequency hiss, *J. Geophys. Res., 77,* 1157, 1972.

Parrot, M., World map of ELF/VLF emissions observed by a low-orbiting satellite, *Ann. Geophys., 8,* 135, 1990.

Sotnikov, V.I. et al. Excitation of sidebands due to nonlinear coupling between a VLF transmitter signal and a natural ELF emission, *J. Geophys. Res., 96,* 11,363, 1991.

Tanaka, Y., D. Lagoutte, M. Hayakawa, F. Lefeuvre and S. Tajima, Spectral broadening of VLF transmitter signal and sideband structure oberved on AUREOL 3 satellite at middle latitudes, *J. Geophys. Res. , 92,* 7551, 1987.

Y. R. Dalkir and M. C. Lee, Plasma Fusion Center, Massachusetts Institute of Technology, Cambridge, Massachusetts 02139.

K. M. Groves, Ionospheric Physics Division, Phillips Laboratory, Hanscom Air Force Base, Massachusetts 01731.

S. P. Kuo, Weber Research Institute, Polytechnic University, Farmingdale, New York 11735.

(received February 10,1992;
revised June 18, 1992;
accepted June 25, 1992)

Paper number 92JA01531.
0148–0227/92/92JA–01531$02.00

DALKIR ET AL.: BRIEF REPORT

DALKIR ET AL.: BRIEF REPORT

Figure 1. Calculated frequency (frequency shift), due to the proposed Doppler shift effect, of the low frequency mode (the symmetric sideband modes) as a function of the ratio of the plasma frequency (ω_{pe}) to the electron cyclotron frequency (Ω_e) when (1) the dominant ion species is H^+ and the incident wave frequency is 11.90 kHz (denoted by the dashed line), (2) the dominant ion species is H^+ and the incident wave frequency is 12.65 kHz (denoted by the full line), (3) the dominant ion species is O^+ and the incident wave frequency is either 11.90 kHz or 12.65 kHz (denoted by the dash-dot line)-no significant difference is found between the results for these two frequencies. At the altitude of 1200 km, the measured ω_{pe}/Ω_e was found to be between 0.7 and 0.8 [*Hoffman and Dodson,* 1980].

Figure 1. Calculated frequency (frequency shift), due to the proposed Doppler shift effect, of the low frequency mode (the symmetric sideband modes) as a function of the ratio of the plasma frequency (ω_{pe}) to the electron cyclotron frequency (Ω_e) when (1) the dominant ion species is H^+ and the incident wave frequency is 11.90 kHz (denoted by the dashed line), (2) the dominant ion species is H^+ and the incident wave frequency is 12.65 kHz (denoted by the full line), (3) the dominant ion species is O^+ and the incident wave frequency is either 11.90 kHz or 12.65 kHz (denoted by the dash-dot line)-no significant difference is found between the results for these two frequencies. At the altitude of 1200 km, the measured ω_{pe}/Ω_e was found to be between 0.7 and 0.8 [*Hoffman and Dodson*, 1980].

Radio Reflectivity of Lightning-Induced Plasmas

Y. R. Dalkir and M. C. Lee
Plasma Fusion Center
Masssachusetts Institute of Technology
Cambridge, MA 02139

E. R. Williams
Center of Meteorology and Physical Oceanography
Massachusetts Institute of Technology
Cambridge, 02139

Submitted to the Journal of Geophysical Research

Abstract

The scattering of radio waves from lightning-induced plasmas is investigated. The plasmas are modeled as long, thin, perfectly conducting vertical channels with surface density irregularities on a scale much smaller than the total channel length. The theoretically predicted wavelength dependence of the radar reflectivity is compared to experimental results obtained with the MIT C-band, S-band, and the Millstone UHF radars. It is found that the rough surface scattering model can adequately account for the $1/\lambda^2$ wavelength dependence of the radar reflectivity observed in the MIT-Millstone Hill experiments, if the density fluctuations of the lightning-induced plasmas have a power-law type spectrum.

1 Introduction

Lightning is a series of short, complex, pulsed electric discharges that create highly irregular plasma strips in the atmosphere. A typical lightning-induced plasma channel is kilometers in length and centimeters to meters in diameter, with a complex dendritic, tortuous structure [Uman, 1969]. Radar lightning studies have been conducted since the 1950's using X-band to UHF radio waves, and extensive data are available in the literature. In particular, the wavelength dependence of the radar reflectivity is of interest, since it is thought to be related to the surface density inhomogeneities of the plasma channels [Lee et al., 1988].

This paper is concerned with a radar lightning study conducted with the MIT S-band, C-band, and the Millstone UHF radars. These experiments demonstrated an overall inverse square dependence between radar reflectivity and wavelength, though the results were highly variable at any one wavelength, and likely to be affected by precipitation masking [Williams, et al., 1989]. Previous theories of lightning backscatter range from modeling the plasma as an overdense radar target, i.e. a perfect conductor [Ligda, 1956; Mazur et al., 1985], to considering it as composed of underdense plasma channels of varying geometries [Atlas, 1958; Hewitt, 1957; Holmes et al., 1980]. None of the published theories, however, adequately accounts for the average inverse square wavelength dependence of the radar reflectivity of the lightning-induced plasmas.

Williams et al. [1989] attempt to resolve these various conflicting theories by presenting a clear case for an overdense plasma, based on observations of temperature in

thundercloud currents and laboratory discharges, together with theoretical calculations of the temperature dependence of the plasma frequency. They conclude that one may safely model the lightning plasmas as perfectly conducting, thin channels of complex geometry. The failure of the existing theories to account for the wavelength dependence of the radar reflectivity may be due to the neglect of the small scale irregularities of the plasma strips in the models. The present study attempts to correct this neglect by investigating the problem of diffuse scattering of electromagnetic waves from an irregular, perfectly conducting plasma surface. The small-scale plasma density irregularities are assumed to have a power-law rather than a Gaussian type spectrum, as suggested by wave propagation studies conducted in both laboratories and in the ionosphere [Lee et al., 1989]. The theoretical wavelength dependence of the reflected power in this model is found to be in good agreement with the observations.

The paper is organized as follows: Section 2 presents a summary of the relevant results obtained in the MIT-Millstone Hill experiments; Section 3 outlines the proposed theory. The assumptions made in the model of radio wave scattering off a plasma strip with density irregularities (viz., rough surface) are further discussed in Section 4. Conclusions follow in Section 5.

2 Experimental Results

The radar lightning experiments were carried out with the S-band (11 cm) and C-band (5.4 cm) radars on the MIT campus, and the steerable 150 foot UHF (68 cm) radar dish operated by the MIT Haystack Observatory at Millstone Hill [Williams et al., 1989: Dalkir et al., 1992]. The radars were pulsed for 1 to 3 μs at repetition rates of between 200 to 900 Hz. The pulse echoes were recorded over a wide range, from a few kilometers up to one hundred, over different storm days. The radar beamwidth was 1.4° for the MIT radars, and 1.0° for the Millstone UHF radar. The S-band and C-band radars were operated with horizontal electric field, while the UHF beam was circularly polarized. All experimental runs were conducted with the radar beams fixed (See Figure 1).

A histogram of the observations, showing the large variability of the volume reflectivity at any one wavelength, may be found in Figure 11 of Williams et al. [1989]. The exact causes of this variability remain unexplained at present, but is likely to be due to the variation in size, shape and location of the lightning-induced plasmas over the course of the experiments. Reflection from the precipitation accompanying the lightning storms, or "precipitation masking", may also effectively reduce the observed wavelength dependence of the backscattered power [Williams et al., 1989]. The mean reflectivity at any one wavelength, however, clearly displays a $1/\lambda^2$ dependence (see Figure 2).

3 Theory

3.1 Radio Reflectivity of Lightning-Induced Plasma Channels

This section outlines the theory of rough surface scatter, as applied to a lightning-induced plasma layer in the atmosphere. The analysis follows the method introduced by M. A. Isakovich (1952), who considered the scattering of sound waves from perfectly reflecting surfaces with randomly distributed irregularities. His method was extended by P. Beckmann and A. Spizzichino (1963) to include electromagnetic wave scattering from perfectly conducting surfaces of varying degrees and types of roughness. The following analysis expands these results by applying them to the specific problem of radar backscatter from lightning-induced plasmas.

Consider the scattering of plane electromagnetic waves with electric field $E_1 e^{i\mathbf{k_1}\cdot\mathbf{r}-i\omega t}$, where $\mathbf{k_1}, \omega$ are the wave vector and angular frequency, respectively, and $\mathbf{r}$ is the position vector with respect to the origin of a cylindrical coordinate system with basis vectors $\mathbf{e_r}, \mathbf{e_\phi}, \mathbf{e_z}$. The scattering plasma surface is most appropriately modeled as a long, thin, rough cylinder, with its axis of symmetry aligned with the z-axis (see Figure 3). The vector $\mathbf{s} = [S + \delta s(z, \phi)]\mathbf{e_r} + z\mathbf{e_z}$ extends from the origin to surface of the plasma. The unperturbed plasma channel has radius S; first-order, random deviations from this are described by the function $\delta s(z, \phi)$. The scattered wave is characterized by the parameters $E_2, \mathbf{k_2}$ and ω.

In this simplified model, only the small-scale density irregularities along any one

section of an approximately vertical lightning channel are considered. The branch-like structure of the plasma channels, or their large-scale deviations from the surface $s = S$ (i.e., any background inhomogeneities), are ignored. Furthermore, since the overdense plasma channels are long and thin, it is reasonable to assume that any density perturbations will have azimuthal symmetry: henceforward we assume $\delta s(z, o) = \delta s(z)$.

The analysis proceeds by use of the Helmholtz integral which describes the total electric field at any point P in terms of the electric field on the scattering surface:

$$E(P) = \frac{1}{4\pi} \int \int [E_A \frac{\partial \Psi}{\partial n} - \Psi \left(\frac{\partial E}{\partial n}\right)_A] dA \tag{1}$$

where $\Psi = e^{ik_2 R'}/R'$, R' is the distance from P to the scattering point, E_A is the electric field on the surface A, and $\mathbf{n}$ is the normal vector to the surface at the scattering point. To deal with plane waves, we consider only the far field, i.e. the point P is distant from the scattering point, such that $k_2 R' \approx k_2 R_0 - \mathbf{k_2} \cdot \mathbf{s}$ and $\Psi \approx \exp(ik_2 R_0 - i\mathbf{k_2} \cdot \mathbf{s})/R_0$ (see Figure 4). Furthermore, we ignore multiple reflection from the rough surface, so that, in the steady state,

$$E_A = (1 + R) E_1 e^{i\mathbf{k_1 s}} \tag{2}$$

$$\left(\frac{\partial E}{\partial n}\right)_A = i(1 - R) E_1 \mathbf{k_1} \cdot \mathbf{n} e^{i\mathbf{k_1} \cdot \mathbf{s}} \tag{3}$$

where R is the reflection coefficient and $\mathbf{n}$ is the local normal to the surface at the scattering point. The reflection coefficient is in general a function of the angle of incidence and polarization of the incident waves, and the electrical properties of the reflecting material.

Equation (2) is a good approximation to the surface field when the radius of curvature of the rough surface is large with respect to the wavelength of the incident wave. i.e. the surface has no sharp edges. The normal derivative of the surface electric field is obtained by considering the reflected and incident waves with respect to the tangent plane to the surface at the scattering point. Equation (3) is valid within the ray approximation. or when edge (diffraction) effects can be ignored. This is the case for $L >> \lambda$. where L represents the characteristic linear size of the scattering surface. and λ is the wavelength of the incident wave. A typical lightning-induced plasma cylinder is kilometers in length and may be meters in diameter, and thus satisfies the condition $L >> \lambda$ in both the $\mathbf{e_r}$ and $\mathbf{e_z}$ directions [Uman, 1969].

Substituting Equations (2) and (3) into the Helmholtz integral (Equation (1)) yields

$$E(P) = \frac{iE_1 e^{ik_2 R_0}}{4\pi R_0} \int\int [R(\mathbf{k_1} - \mathbf{k_2}) \cdot \mathbf{n} - (\mathbf{k_1} + \mathbf{k_2}) \cdot \mathbf{n}] e^{i(\mathbf{k_1} - \mathbf{k_2}) \cdot \mathbf{s}} dA \qquad (4)$$

It is convenient to consider the normalized electric field $\hat{E} = E/[iE_1 e^{ik_2 R_0}/4\pi R_0]$. Furthermore, $\mathbf{k_2} = -\mathbf{k_1}$, since monostatic, diagnostic radars were used in the experiments. Equation (4) can thus be rewritten as:

$$\hat{E} = 2R \int\int \mathbf{k} \cdot \mathbf{n} e^{i2\mathbf{k} \cdot \mathbf{s}} dA \qquad (5)$$

where $\mathbf{k} = \mathbf{k_1}$; R, the local reflection coefficient at each scattering point, has been aproximated to be constant over the entire surface. This is appropriate for the lightning-induced plasmas, which are almost perfectly conducting, i.e. $|R| \approx 1$ [Williams et al., 1989].

The surface element and normal vector can be written in terms of the density perturbation $\delta s(z)$ as:

$$dA = Sd\phi dz\sqrt{1+(\delta s')^2} \tag{6}$$

$$\mathbf{n} = (-\delta s'\mathbf{e_z} + \mathbf{e_r})\sqrt{1+(\delta s')^2}$$

where $\delta s' = \partial(\delta s)/\partial z$. Substituting these terms into Equation (5) yields

$$\hat{E} = 2R\int_0^{\pi} Sd\phi \int_{-h/2}^{h/2} dz[-k_z\delta s' + k_r]e^{i2[k_z z + k_r \delta s(z) + k_r S]} \tag{7}$$

where h is the characteristic height of the scattering cylinder.

After performing the integration over ϕ, and integrating the term $-k_z\delta s' e^{i2k_r\delta s}e^{i2k_z z}$ by parts, Equation (7) becomes

$$\hat{E} = 4Re^{iS2k_r}\pi S\Big[(\frac{k_r^2+k_z^2}{k_r})\int_{-h/2}^{h/2} dz e^{2i[k_z z + k_r y\delta s(z)]} - 4R\frac{k_z}{k_r}\sin(k_z h)\Big] \tag{8}$$

where for simplicity we have assumed that the surface is fixed at the edges; i.e. $\delta s(h/2) = \delta s(-h/2) = 0$. The contribution of the second term to the scattered power is small compared to the first, as may be verified by retaining it throughout the analysis; in the interest of simplicity, it will be neglected.

The mean scattered power can be expressed as $< P >= (1/2) < E E^* > /\eta_0$ where η_0 is the intrinsic impedance of the propagation medium; $\eta_0 = 120\pi \sim 377\ (\Omega)$ for free space. From Equation (8), we may write

$$< \hat{E}\hat{E}^* >= 4\pi^2 S^2 \frac{(k_r^2+k_z^2)^2}{k_r^2}\int_{-h/2}^{h/2} dz_1 \int_{-h/2}^{h/2} dz_2 e^{i2k_z(z_1-z_2)} < e^{i2k_r[\delta s(z_1)-\delta s(z_2)]} > \tag{9}$$

where we have taken $R^2 = 1$.

To proceed further, one must adopt a specific model for the roughness parameter $\delta s(z)$. Plasma irrregularities created by lightning are unlikely to have a periodic or

similarly deterministic structure: rather, noise-like, random perturbations are expected. We therefore model the extent of the plasma in the r direction as a random variable $\delta s(z)$, which is completely described by a Gaussian joint probability density function $f[\delta s(z_1), \delta s(z_2)]$ with standard deviation σ, and a normalized autocorrelation function $C(|z_1 - z_2|)$ with characteristic length l and index m:

$$f[\delta s(z_1), \delta s(z_2)] = \frac{1}{2\pi\sigma^2\sqrt{1-C^2}} \exp(-\frac{\delta s(z_1)^2 - 2C\zeta(z_1)\delta s(z_2) + \delta s(z_2)^2}{2\sigma^2(1-C^2)}) \qquad (10)$$

$$C(|z_1 - z_2|) = \exp(-|z_1 - z_2|^m / l^m) \qquad (11)$$

Physically, σ and l characterize the height and size of the irregularities of the lightning-induced plasma. Any roughness profile can be approximated by varying the parameters of the joint probability distribution and the autocorrelation function: a large value of σ and a small l imply highly localized peaks with large density variations; by contrast, small σ and large l imply generally low, wide irregularities (see Figure 3). In order to realistically ignore multiple reflections in the model, we have assumed the absence of sharp peaks in the roughness distribution on the surface of the perfectly conducting, lightning-induced plasma; this requirement is satisfied in the regime $l >> \lambda$, $l > \sigma$. Previous authors have concentrated on Gaussian spectra (i.e. $m = 2$ in Equation (11)) [Isakovich, 1952; Beckmann and Spizzichino, 1963]; studies of transionospheric radio wave propagation have shown, however, that power-law type spectra provide the more realistic model for plasma irregularities [Lee et al., 1989, and references therein]. We therefore take $m = 1$ for the function given in Equation (11).

The definition of the mean in Equation (9) can then be rewritten in terms of the probability density functions as:

$$< e^{2ik_r(\zeta(z_1)-\zeta(z_2))} >= \int_{-\infty}^{\infty} dz_1 \int_{-\infty}^{\infty} dz_2 f(z_1, z_2) e^{2ik_r(z_1-z_2)} \equiv \chi_2(2k_r, -2k_r) \qquad (12)$$

where χ_2 is the two-dimensional characteristic function of the joint probability distribution $f(z_1, z_2)$. Similarly, the one-dimensional characteristic function is defined as

$$\chi(2k_r) \equiv < e^{2ik_r z} >= \int_{-\infty}^{\infty} f(z) e^{i2k_r z} dz \qquad (13)$$

where $f(z) = (\sqrt{2\pi}\sigma)^{-1} \exp(-z^2/2\sigma^2)$. It is useful to first calculate the variance, $\mathrm{d}(\hat{E}) = < \hat{E}\hat{E}^* > - < \hat{E} >< \hat{E} >^*$, given by

$$d(\hat{E}) = 4\pi^2 S^2 \frac{(k_r^2 + k_z^2)^2}{k_r^2} \int_{-h/2}^{h/2} dz_1 \int_{-h/2}^{h/2} dz_2 e^{i2k_z(z_1-z_2)} [\chi_2(2k_r, -2k_r) - \chi(2k_r)\chi^*(2k_r)] \qquad (14)$$

For a Gaussian joint probability distribution function, $\chi(2k_r) = exp(-2k_r^2\sigma^2)$ and $\chi_2(2k_r, -2k_r) = \exp[-4k_r^2\sigma^2(1-C)]$; thus Equation (14) becomes

$$d(\hat{E}) = 4\pi^2 S^2 \frac{(k_r^2 + k_z^2)^2}{k_r^2} \int_{-h/2}^{h/2} dz_1 \int_{-h/2}^{h/2} dz_2 e^{i2k_z(z_1-z_2)} [e^{-4k_r^2\sigma^2(1-C)} - e^{-4k_r^2\sigma^2}] \qquad (15)$$

The integrand vanishes when $C = 0$, or when $|z_1 - z_2|$ is large; thus we may appoximate $C = \exp(-|z_1 - z_2|)/l \approx 1 - |z_1 - z_2|/l$ and replace the integration limits for z_2 by $z_1 \pm l \geq z_2$, where l is the maximum range of $|z_1 - z_2|$ for which the first order approximation to the exponential is valid. Thus Equation (15) can be expressed as

$$d(\hat{E}) = 4\pi^2 S^2 \frac{(k_r^2 + k_z^2)^2}{k_r^2} \int_{-h/2}^{h/2} dz_1 \int_{z_1-l}^{z_1+l} dz_2 e^{i2k_r(z_1-z_2)} [e^{-4k_r^2\sigma^2(|z_1-z_2|/l)} - e^{-4k_r^2\sigma^2}] \qquad (16)$$

This is a good approximation to the variance insofar as the integrand in Equation (15) is localized within $\pm l$; it can be seen that this is the case for a very rough surface, i.e.: $4k_r^2\sigma^2 >> 1$, which is the relevant regime for the lightning backscatter experiments considered here (see Section 3.1.1). Integrating the expression in Equation (16) yields the following final result:

$$< \hat{E}\hat{E}^* >= d(\hat{E}) + < \hat{E} >< \hat{E} >^* \tag{17}$$

$$= 4h\pi^2 S^2 \frac{(k_r^2 + k_z^2)^2}{k_r^2}\Big[\frac{8k_r^2\sigma^2/l}{16k_r^4\sigma^4/l^2 + 4k_z^2} - 2e^{-4k_r^2\sigma^2}\ \mathrm{Re}\Big[\frac{e^{i2k_z l}}{4k_r^2\sigma^2/l - i2k_z}\Big]$$

$$-e^{-4k_r^2\sigma^2}\sin(2k_z l)/k_z + e^{-4\sigma^2 k_r^2}\sin^2(k_z h)/(k_z^2 h)\Big]$$

where Re means the real part; the quantity $< \hat{E} >< \hat{E} >^*$ has been calculated directly from Equations (8) and (13). Neglecting terms on the order of $e^{-4k_r^2\sigma^2}$ yields:

$$< P > \propto < \hat{E}\hat{E}^* > \approx 32h\pi^2 S^2 \frac{(k_r^2 + k_z^2)^2}{k_r^2}\Big[\frac{k_r^2\sigma^2/l}{16k_r^4\sigma^4/l^2 + 4k_z^2}\Big] \tag{18}$$

The term $(k_r^2 + k_z^2) = k^2 - k_\phi^2$ indicates that $< P >= 0$ for $k = k_\phi$; i.e. the backscattered power is zero for grazing incidence of the radio waves on the plasma cylinders, as expected.

3.1.1 Comparison to Experimental Results

Figure 3 illustrates the scenario of a typical experimental run: the transmitting radar may be located tens of kilometers from the lightning bolts, which extend more or less vertically through the atmosphere for an average of ten kilometers for cloud to ground lightning [Uman, 1969]. A long cylindrical plasma channel is generated around the

lightning discharge, with first order random irregularities extending orthogonally to the surface. Observations of the luminous core of the plasma indicate typical diameters of 1 cm or less, where the lightning arc temperature may exceed 5000°K for tens of milliseconds [Williams et al., 1989]. This corresponds to electron densities of between 10^{19}-10^{20} m^{-3}, indicating that the core of the plasma is overdense to incident radio frequencies of up to approximately 80 GHz. An electron density of one order of magnitude less would still be overdense to the radio frequencies used in the MIT-Millstone experiments. Thus the effective scattering region is expected to extend to radii larger than the luminous core, where a cooler, less dense plasma has been formed. Previously reported photographic observations and theoretical calculations predict plasma channel radii on the order of meters [Uman, 1969, and references therein]. Thus we expect the effective overdense plasma cylinders to be kilometers long and meters in diameter.

The height (σ) of the surface density irregularities of these plasma cylinders cannot be directly observed, since they occur in the non-luminous outer regions of the plasma. Based on the expected dimensions of the plasma tubes, however, one may reasonably estimate the standard deviation σ to be on the order of tens of centimeters, and the outer scale length of the irregularity spectrum or autocorrelation distance l to be on the order of meters. This satisfies the required conditions that the surface density irregularities be smooth, i.e. $l >> \lambda$ and $\sigma < l$. Under these conditions, it can be shown that $k_z^2 > 4k_r^4\sigma^4/l^2$, and thus the mean backscattered power in Equation (18) can be

approximated as

$$< P > \approx h\frac{S^2}{\pi^2}\frac{\sigma^2}{2l}\frac{(k_r^2 + k_z^2)^2}{k_z^2} \propto 1/\lambda^2 \tag{19}$$

The last proportionality is true since the angle of incidence (θ) of the radio waves on the scattering surfaces is not expected to vary significantly over the course of the experiments (see Figure 3).

The full range of validity of Equation (19) must be carefully examined. The result may be applied only where the approximation used in evaluating the integral in Equation (15) is justified; this is the case for $4k_r^2\sigma^2 >> 1$. Equation (19) is valid only in the limit $k_z^2 >> 4k_r^4\sigma^4/l^2$. Furthermore, multiple reflections from the scattering surface may be ignored only insofar as the density irregularities are smooth; this condition is met when $l >> \lambda$. The various requirements for which Equation (19) is valid may therefore be summarized as follows: $4k_r^2\sigma^2 >> 1$; $k_z^2 >> 4k_r^4\sigma^4/l^2$ and $\lambda << l$. These bounds may be written in terms of the angle of incidence of the radio waves as $4\pi\cos\theta > \lambda/\sigma > (\sigma/l)4\pi(\cos\theta/\tan\theta)$; $\lambda/\sigma << l/\sigma$, where for simplicity we have assumed that $k_\phi = 0$. Figures 5a and 5b illustrate these relations for two different values of σ/l. It can be seen that the region of validity of Equation (19) is relatively large and sensitive to the exact value of the dimensions of the surface irregularities.

The geometry illustrated in Figure 3 indicates that large angles of incidence ($\theta > 45°$) are expected in the experiments. Intracloud lightning discharges are far more common than cloud-to-ground lightning; the radio waves are more likely to be scattering off plasma channels that are generated high above the ground. If we estimate $\theta \approx 60°$, on

average, Figure 4b indicates that the analysis is valid only in the regime $0.5 < \lambda/\sigma < 6$. This condition is indeed satisfied for the estimated sizes of the density irregularities ($\sigma \approx$ 10 cm; $l \approx 2$ m).

The one-dimensional model adopted in the analysis, i.e. $\delta s(z, \phi) = \delta s(z)$ is appropriate for the lightning-created plasmas, which are long cylinders aligned with the z-axis (see Figure 4). The random density fluctuations of the plasma in the r-direction are thus expected to depend only on the z-coordinate of the surface, and not vary significantly with azimuth. Since the length (h) of the lightning-induced plasma strips is very long (on the order of a few kilometers), the other conditions assumed in the analysis , i.e. $\lambda << l << h$, are reasonably met for all three frequencies used in the experiments.

The experimental data shown in Figure 2 are thus within the regime of validity of Equation (19), which predicts an inverse square power law dependence between the backscattered power and the incident wavelength. The actual line of best fit for the experimental data indeed show an inverse square dependence of the power on the radar wavelength, which is in good agreeement with the theoretical result of Equation (19). It should be stressed that the relation $< P > \propto 1/\lambda^2$ in Equation (19) only holds for plasma density irregularities with a power-law spectrum whose correlation function is given by Equation (11) with $m = 1$. Both laboratory and ionospheric studies of turbulent plasmas indicate that density perturbations are best modeled by these types of spectra [Lee, et al., 1989]. A Gaussian spectrum for the density irregularities, by contrast, leads to $< P > \propto 1/\lambda$, which does not agree with the observations.

4 Conclusions

The wavelength dependence of the backscattered power from lightning-induced plasmas has been studied in experiments conducted with the MIT S-band, C-band, and the Millstone UHF radars. The average reflected power was observed to decrease with the wavelength as $1/\lambda^2$. This behavior can be successfully explained by the scattering of electromagnetic waves from the small-scale density irregularities of the lightning-induced, perfectly conducting plasma channels in the atmosphere. These density irregularities are reasonably assumed to have a power-law rather than a Gaussian spectrum. A region of validity for the predicted $1/\lambda^2$ relation is believed to exist in the experiments, which depends on the expected size of the density irregularities (σ/l), and the angle of incidence of the radio waves on the plasma channels.

Acknowledgments. This work is supported by NSF Grant No. ATM-9016235 and AFOSR Grant No. F49620-92-J-0103 and Grant No. AFOSR-92-0001.

References

Atlas, D., Radar lightning echoes and atmospherics in vertical crossection, *Recent Advances in Atmospheric Electricity,* L.G. Smith, editor, Pergamon Press, 1958.

Beckmann, P., and A. Spizzichino, *The Scattering of Electromagnetic Waves from Rough Surfaces,* Pergamon Press, New York, 1963.

Dalkir, Y.R., M.C. Lee, E.R. Williams, Radio Reflectivity of lightning-induced plasmas, to be submitted to JGR for publication.

Gurevich, A.V., An ionized layer in a gas (in the atmosphere), *Sov. Phys. Usp., 23,* 862, 1980.

Hewitt, F.J., Radar echoes from interstroke processes in lightning, *Proc. Phys. Soc. London, B, 70* , 961, 1957.

Holmes, C. R. , E.W. Szymanski, S.J. Szymanski, and C. B. Moore, Radar and acoustic study of lightning, *J. Geophys. Res., 85,* 7517, 1980.

Isakovich, M. A., The scattering of waves from a statistically rough surface (in Russian), *Zhurn. Eksp. Teor. Fiz., 23,* 305, 1952.

Kuo, S.P., Y.S. Zhang, M.C. Lee, P.A. Kossey, and R.J. Barker, An experimental study of OTH radar using Bragg reflection from artificially ionzied layers of a gas, to appear in Radio Sci., 1992.

Lee, M.C., D. Thurairatnam, and E.R. Williams, Radio wave scattering from artificial plasma layers, paper presented at URSI/National Radio Science Meeting, Boulder, CO, Jan., 1988.

Lee, M.C., S. V. Nghiem, and C. Yoo, Effects of irregularity anisotropy on Faraday polarization fluctuations, *J. Geophys. Res., 94,* 15,421, 1989.

Ligda, M.G.H., Lightning detection by radar, *J. Atmos. Terr. Phys.* , *9,* 329, 1956.

Mazur, V., D. S. Zrnic, and W.D. Rust, Lightning channel properties determined with a vertically pointing Doppler radar, *J. Geophys. Res., 90,* 6165, 1985.

Williams, E.R., S.G. Geotis, and A.B. Bhattacharya, A radar study of the plasma and geometry of lightning, *J. Atmos. Sci., 46,* 1173, 1989.

Figure Captions

Fig. 1. Schematic representation of lightning backscatter experiments. The plasma cylinders created through air breakdown around the lighning discharges is diagnosed with the MIT C-band. S-band and Millstone UHF radars. For simplicity, only one lightning discharge is shown: in actuality, the experiments were carried out separately in different electrical storms.

Fig. 2. Summary of experimental results. The average volume reflectivity at $\lambda = 5.4$, 11 and 68 cm is plotted. The numbers in parentheses indicate the number of data points collected. The wavelength dependence predicted by the theory of long thin conductors, and underdense plasma channels is also indicated on the figure. Neither existing model fits the data of the present study, which exhibit a clear $1/\lambda^2$ dependence.

Fig. 3. Schematic representation of overall scattering geometry. The transmitter is located a few kilometers from the lightning activity. Radio signals with wave vector **k** are incident on the plasma surface at an angle θ to the horizontal. The **z** axis is taken to along the axis of symmetry of the plasma channel, which is approximately perpendicular to the ground. The position vector **s** extends from the origin of the coordinate system to the surface of the lightning-induced plasma; **n** is the local normal vector to the surface. h is the vertical extent of the plasma, which is estimated to be on the order of kilometers.

Fig. 4. Section of lightning-induced plasma, showing smooth surface irregularities with characteristic parameters σ and l (figure not drawn to scale). The geometry illustrates the relation $k_2 R' = k_2 R_0 - \mathbf{k_2} \cdot \mathrm{s}$ used after Equation (1).

Fig. 5a. Plot showing region of validity of $1/\lambda^2$ dependence of backscattered power (Equation (19)). The quantity λ/σ must lie in the region bounded by the curves $4\pi \cos\theta$, $4\pi(\sigma/l)(\cos\theta/\tan\theta)$ and $\lambda/\sigma = 10$ for the approximations made in the analysis to be valid. The value of σ/l has been taken to be 0.1.

Fig. 5b. The plot of Fig. 5a is repeated for $\sigma/l = 0.05$. The upper bound is now given by $\lambda/\sigma = 20$, which is above the point of intersection of the lower bounds.

Figure 1

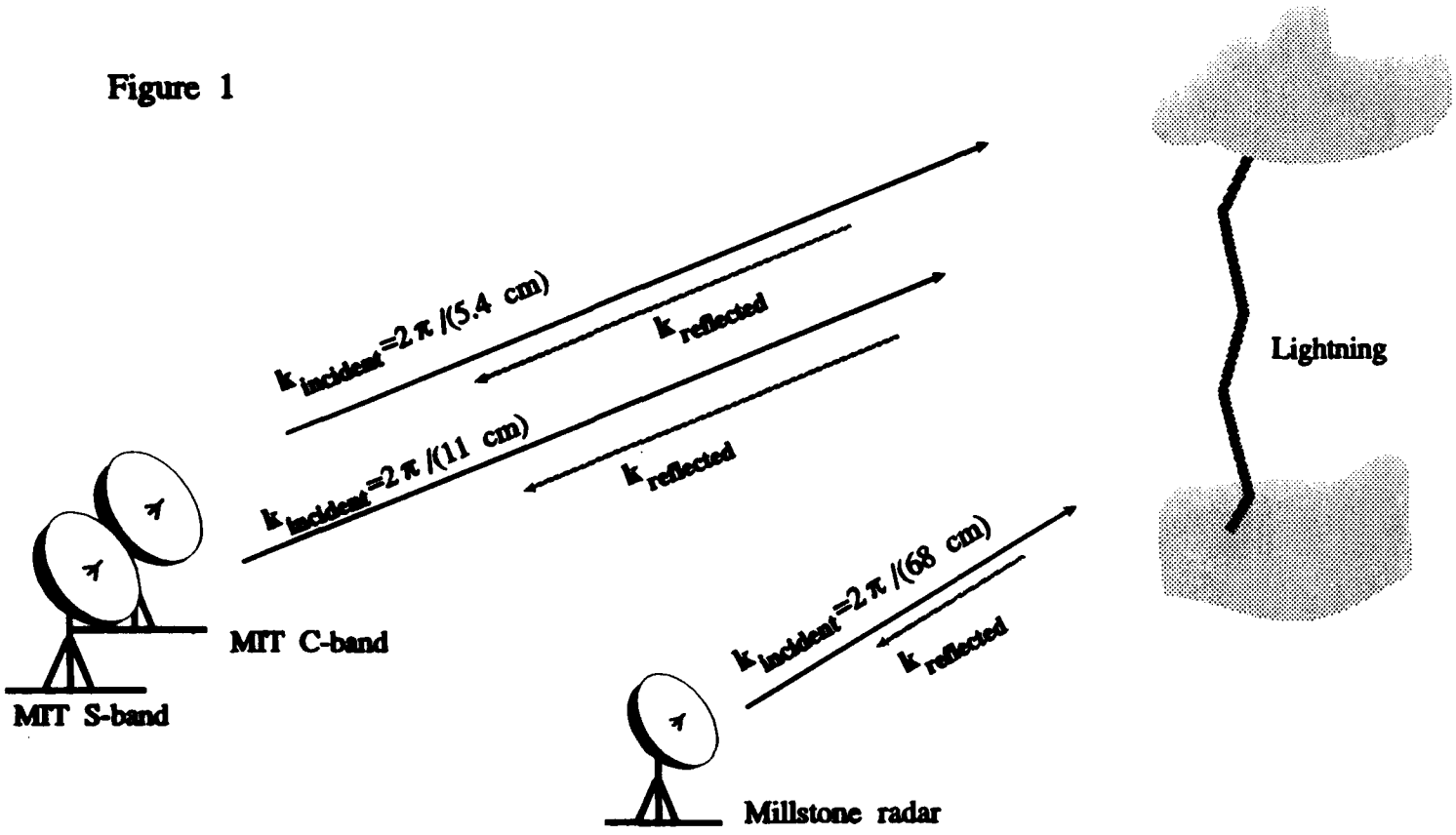
$k_{incident}=2\pi/(5.4\ cm)$
$k_{reflected}$
$k_{incident}=2\pi/(11\ cm)$
$k_{reflected}$
$k_{incident}=2\pi/(68\ cm)$
$k_{reflected}$
Lightning
MIT C-band
MIT S-band
Millstone radar

Figure 2

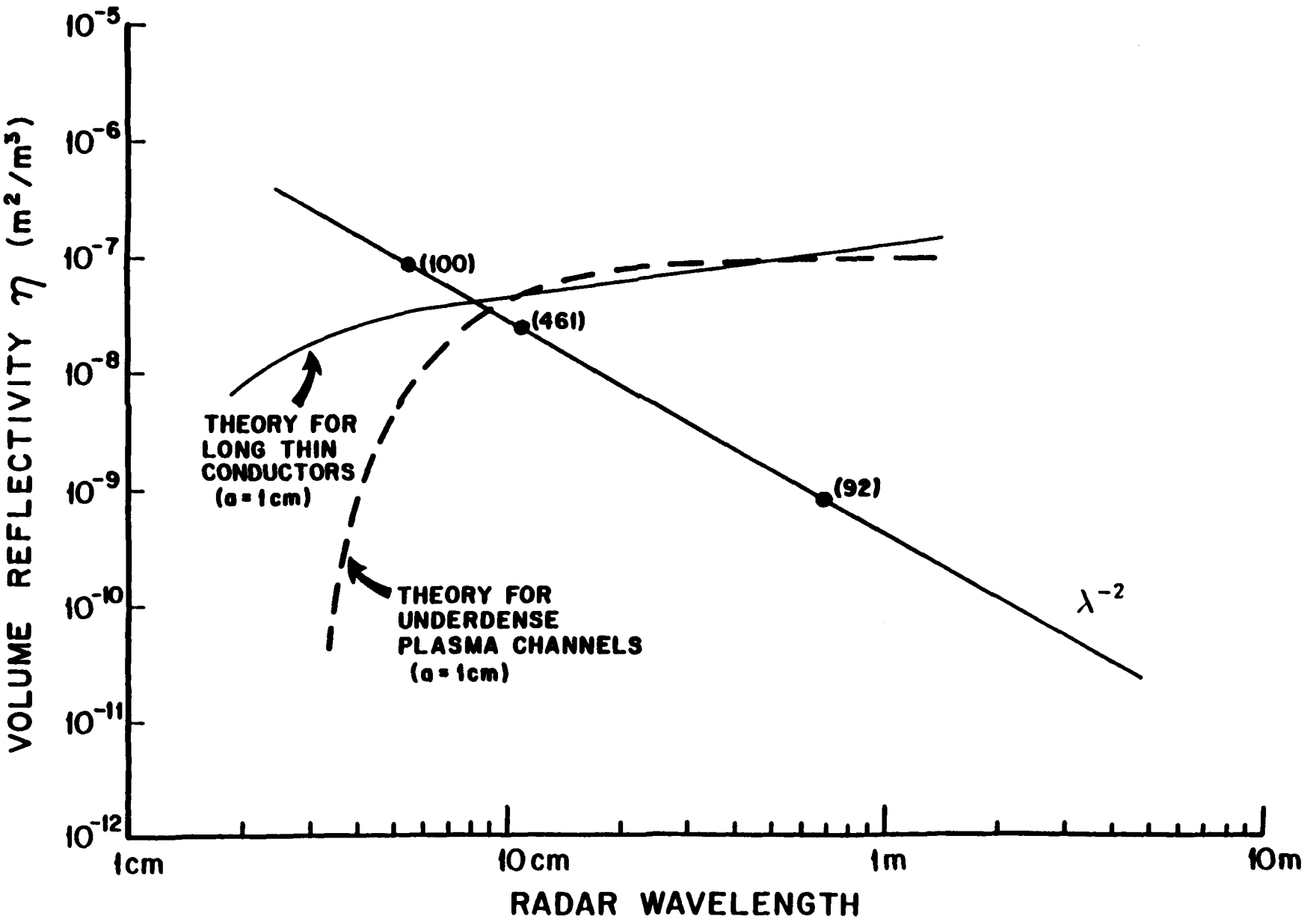
VOLUME REFLECTIVITY η (m²/m³)
10⁻⁵
10⁻⁶
10⁻⁷
10⁻⁸
10⁻⁹
10⁻¹⁰
10⁻¹¹
10⁻¹²
(100)
(461)
(92)
THEORY FOR LONG THIN CONDUCTORS (a = 1cm)
THEORY FOR UNDERDENSE PLASMA CHANNELS (a = 1cm)
λ⁻²
1cm
10cm
1m
10m
RADAR WAVELENGTH

Figure 3

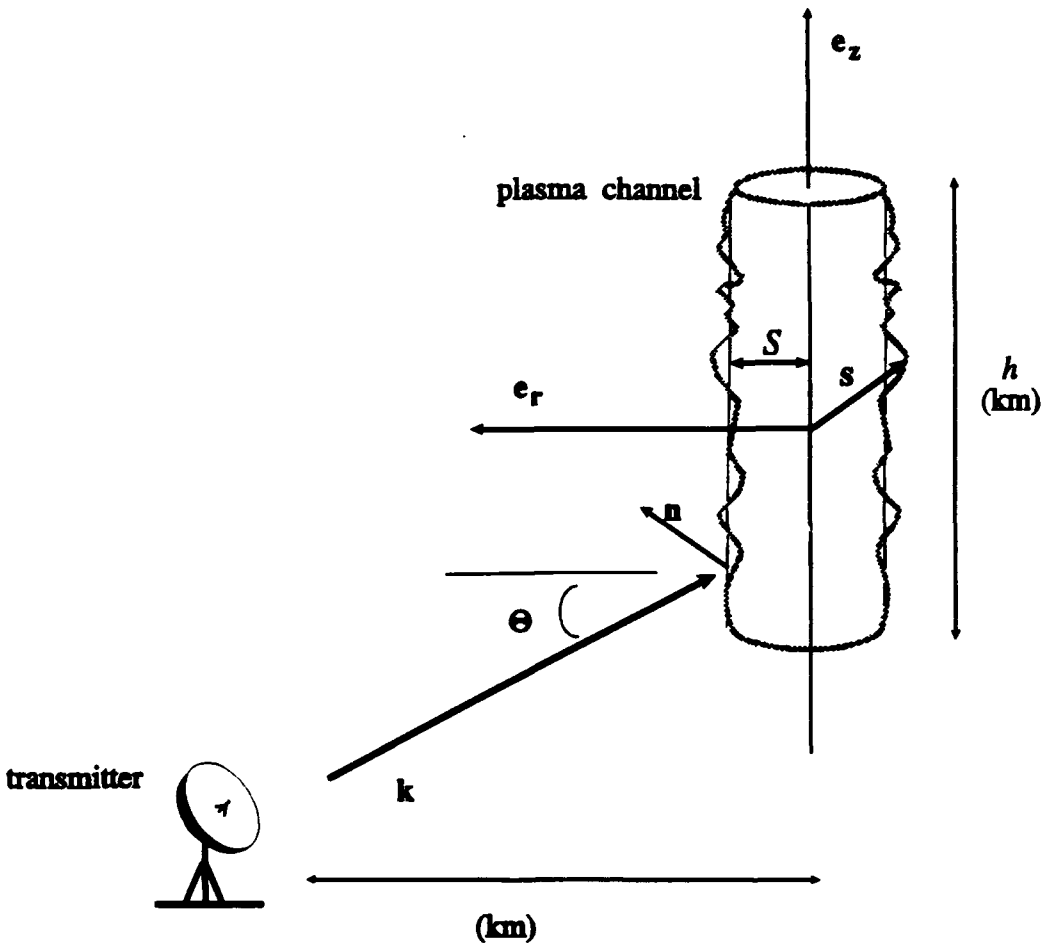

Figure 4

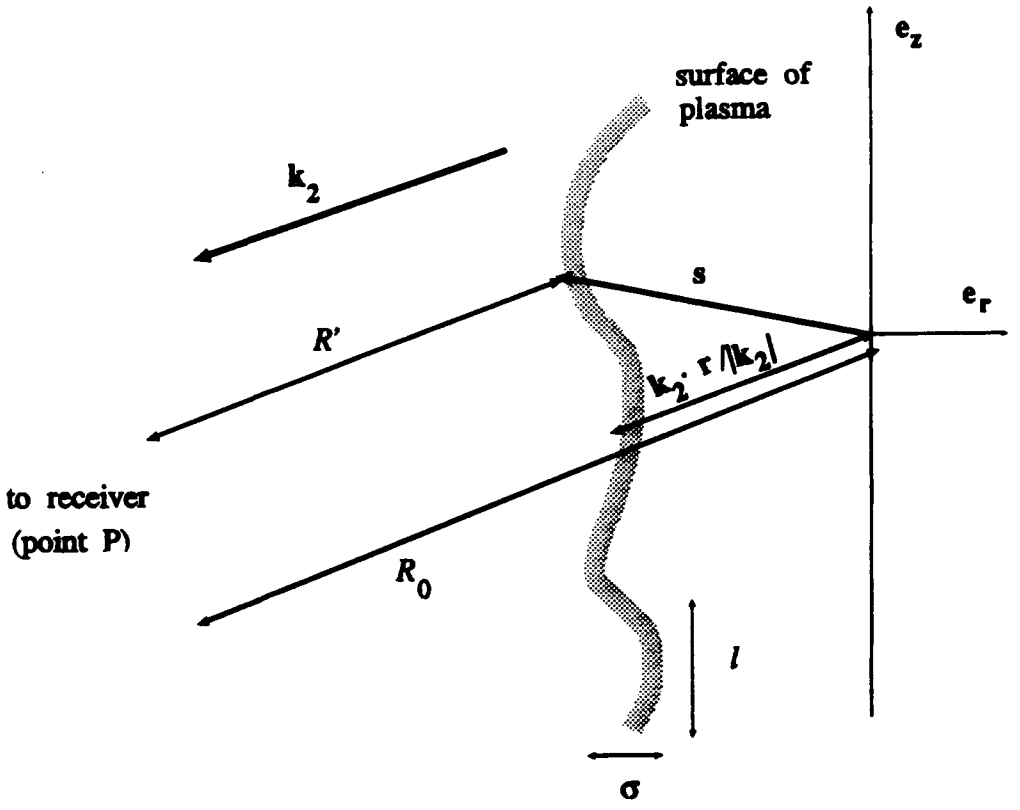
e_z
surface of plasma
k_2
s
e_r
R'
$k_2 \cdot r/|k_2|$
to receiver (point P)
R_0
l
σ

Figure 5a

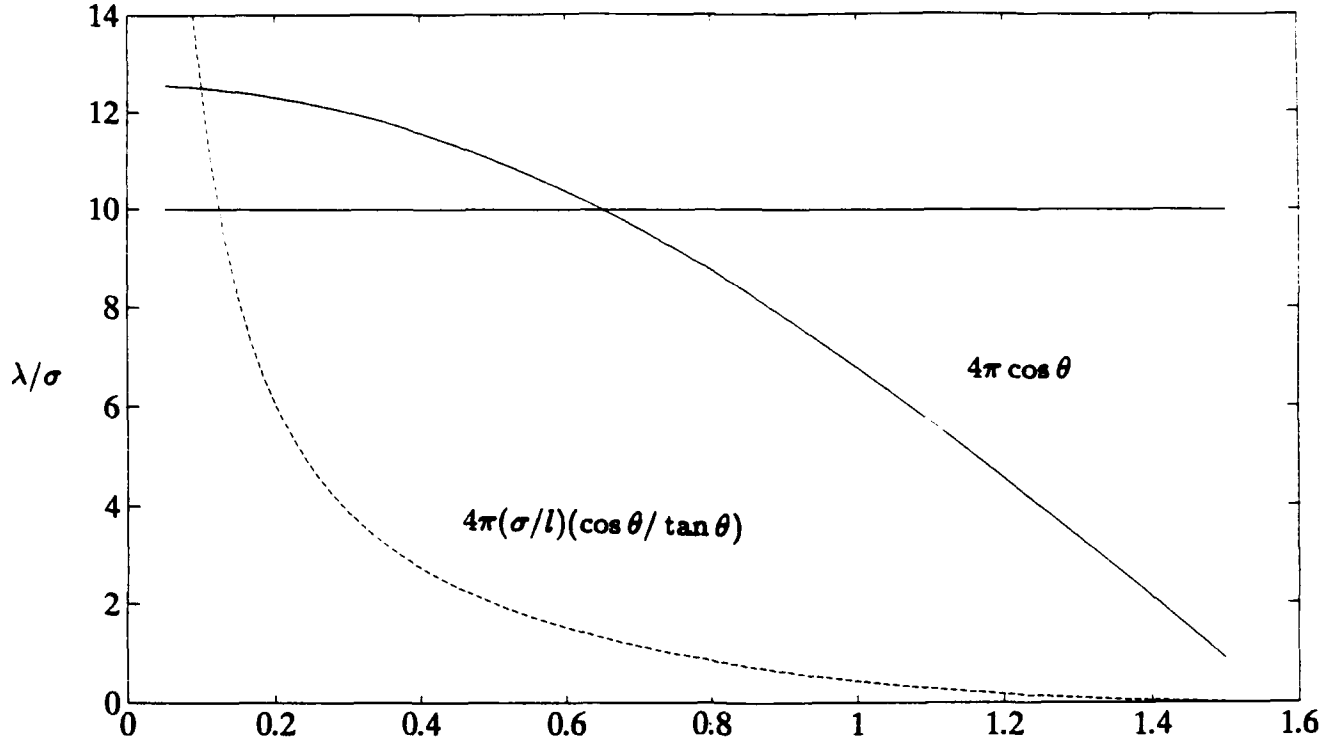

Figure 5b

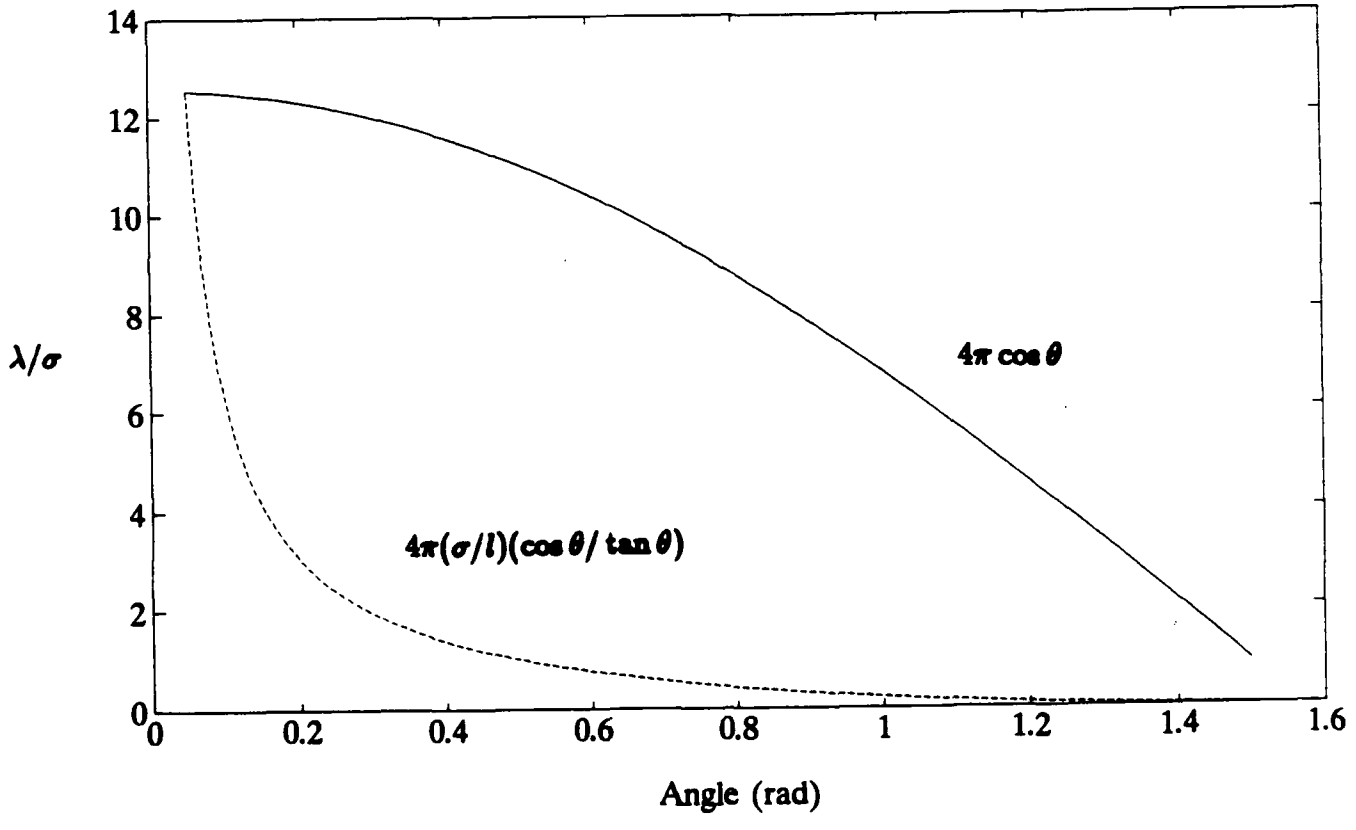

Radar Studies of Lightning-Induced Plasmas with Potential Applications to Radio Communications and Space Surveillance

Y. R. Dalkir and M. C. Lee
Plasma Fusion Center
Department of Electrical Engineering and Computer Science
Masssachusetts Institute of Technology
Cambridge, MA 02139

Submitted to Radio Science

Abstract

The problem of radio backscatter from lightning-induced plasmas is briefly reviewed. The predicted wavelength dependence of the backscattered power is compared to observations made with the MIT S-band, C-band and the Millstone UHF radar. The analysis is extended to plasma disks created through single radar beam heating of the atmosphere. The artificial plasmas are modeled as perfectly conducting, rough plasma pancakes, with random surface inhomogeneities described by either by Gaussian or power-law type spectrum. Only the limiting case where the angle of incidence of the radio waves with respect to the plasma surface is large is considered. In radio communication and space surveillance applications, the reflectivity of the plasma pancakes may be independent of incident wavelength, if the surface density inhomogeneities are characterized by an azimuthally symmetric power law type spectrum. By contrast, a wavelength dependence is expected in diagnostic applications.

1 Introduction

Radio wave reflection from the ionosphere has long been used to extend radio communication paths around the world. The daytime F peak electron densities may vary between 10^5-10^6 cm^{-3}, corresponding to plasma frequencies of between 3-10 MHz. The ionosphere may therefore reflect only HF and lower frequency waves. With the goal of extending radio communication capabilities to higher frequencies, radio scientists have been investigating the possibility of creating high-density, artificial plasma patches in the atmosphere. In one proposed scheme, two very powerful crossed microwave or radio wave beams are employed to produce thin plasma layers through air breakdown in the overlapping beam regions [A.V. Gurevich, 1980; Kuo et al., 1992]. In other proposals, a single radio beam is used to "paint" thin plasma patches in the shape of the beam cross-section in the ionosphere [Short et al., 1991]. Transmitters with power on the order of gigawatts may produce plasma patches dense enough to reflect radio waves with frequencies of up to 1-2 GHz, thus extending radio communication capabilities by two orders of magnitude in frequency over the natural ionosphere.

Important theoretical considerations arise in the design of these artificial communication paths. The effects of surface irregularities on the reflectivity of the plasma patches is of particular interest, since they may impose limitations on the efficiency of radio wave reflection. Scattering from the plasma layers created in the crossed beam technique is essentially a Bragg scattering process, and thus unlikely to be affected significantly by the small surface density irregularities along each layer [Kuo et al., 1992]. By contrast, reflection from the single beam produced "pancake" plasmas is likely to be significantly affected by the surface roughness of the plasma.

Electric storms provide a natural laboratory for testing the effects of surface irregularities

on the radio reflectivity of plasma patches in the atmosphere. Lightning is a series of short, complex, pulsed electric discharges that create highly irregular, dense plasma tubes. Lightning backscatter experiments conducted with the MIT S-band, C-band and the Millstone UHF radar demonstrated an overall inverse square dependence of the radar reflectivity on the incident wavelength [Williams, et al, 1991]. This behavior may be successfully explained by a rough surface scattering model of the lightning-induced plasma cylinders [Dalkir, et al,].

This paper briefly reviews the lightning backscatter experiments and the rough surface scattering model that may account for the inverse square wavelength dependence of the radio wave reflectivity. A similar model of rough surface scattering is then applied to the problem of radio reflection from single radio beam induced, pancake-shaped plasmas. Both bistatic and monostatic radar geometries are analyzed. In radio communication applications, it is found that the surface density irregularities of the artificially induced plasmas may introduce a wavelength dependence into the radio reflectivity, if the spectrum of the density irregularities is Gaussian.

This paper is organized as follows: Section 2 summarizes the MIT-Millstone lightning backscatter experiments; the theory of rough surface radio wave scattering from lightning-induced plasma channels is outlined in Section 3. Section 4 describes the application of the analysis to radar scattering from single beam radio wave induced plasma disks. Conclusions follow in Section 5.

2 Experimental Results

Lightning backscatter experiments were carried out with the S-band (11 cm) and C-band (5.4 cm) radars on the MIT campus, and the steerable 150 foot UHF (68 cm) radar dish operated

by the MIT Haystack Observatory at Millstone Hill [Williams et al., 1989; Dalkir et al., 1992]. The radars were pulsed for 1 to 3 μs at repetition rates of between 200 to 900 Hz. The pulse echoes were recorded over a wide range, from a few kilometers up to one hundred, over different storm days. The radar beamwidth was 1.4° for the MIT radars, and 1.0° for the Millstone UHF radar. The S-band and C-band radars were operated in horizontally polarized mode, while the UHF beam was circularly polarized. All experimental runs were conducted with the radar beams fixed.

Figure 1 displays the reflectivity of the plasma at the three different wavelengths, averaged over numerous individual measurements. The mean reflectivity is clearly characterized by a $1/\lambda^2$ dependence.

3 Rough Surface Scattering Model of Lightning Backscatter

This section outlines the theory of rough surface scatter, as applied to a lightning-induced plasma layer in the atmosphere. The analysis follows the method introduced by M. A. Isakovich (1952), and later extended by P. Beckmann and A. Spizzichino (1963).

Consider the scattering of plane electromagnetic waves with electric field $E_1 e^{i\mathbf{k_1}\cdot\mathbf{r}-i\omega t}$, where $\mathbf{k_1}$, ω are the wave vector and angular frequency, respectively, and $\mathbf{r}$ is the position vector with respect to the origin of a cylindrical coordinate system with basis vectors $\mathbf{e_r}, \mathbf{e_\phi}, \mathbf{e_z}$. The scattering plasma surface is most appropriately modeled as a long, thin, rough cylinder, with its axis of symmetry aligned with the z-axis (see Figure 2). The vector $\mathbf{s} = [S + \delta s(z, \phi)]\mathbf{e_r} + z\mathbf{e_z}$

extends from the origin to surface of the plasma. The unperturbed plasma channel has radius S; first-order, random deviations from this are described by the function $\delta s(z, \phi)$. The scattered wave is characterized by the parameters $E_2, \mathbf{k_2}$ and ω.

In this simplified model, only the small-scale density irregularities along any one section of an approximately vertical lightning channel are considered. It is reasonable to assume that any density perturbations will have azimuthal symmetry, since the overdense plasma channels are long and thin; henceforward we assume $\delta s(z, \phi) = \delta s(z)$.

The analysis proceeds by use of the Helmholtz integral which describes the total electric field at any point P in terms of the electric field on the scattering surface:

$$E(P) = \frac{1}{4\pi} \int \int [E_A \frac{\partial \Psi}{\partial n} - \Psi \left(\frac{\partial E}{\partial n}\right)_A] dA \tag{1}$$

where $\Psi = e^{ik_2 R'}/R'$, R' is the distance from P to the scattering point, E_A is the electric field on the surface A, and $\mathbf{n}$ is the normal vector to the surface at the scattering point. To deal with plane waves, we consider only the far field, i.e. the point P is distant from the scattering point, such that $k_2 R' \approx k_2 R_0 - \mathbf{k_2} \cdot \mathbf{s}$ and $\Psi \approx \exp(ik_2 R_0 - i\mathbf{k_2} \cdot \mathbf{s})/R_0$ (see Figure 3). Furthermore, we ignore multiple reflection from the rough surface, so that, in the steady state,

$$E_A = (1 + R) E_1 e^{i\mathbf{k_1 s}} \tag{2}$$

$$\left(\frac{\partial E}{\partial n}\right)_A = i(1 - R) E_1 \mathbf{k_1} \cdot \mathbf{n} e^{i\mathbf{k_1} \cdot \mathbf{s}} \tag{3}$$

where R is the reflection coefficient and $\mathbf{n}$ is the local normal to the surface at the scattering point. The reflection coefficient is in general a function of the angle of incidence and polarization of the incident waves, and the electrical properties of the reflecting material.

Equation (2) is a good approximation to the surface field when the radius of curvature of the rough surface is large with respect to the wavelength of the incident wave, i.e. the surface has no sharp edges. The normal derivative of the surface electric field is obtained by considering the reflected and incident waves with respect to the tangent plane to the surface at the scattering

point. Equation (3) is valid within the ray approximation, or when edge (diffraction) effects can be ignored. This is the case for $L >> \lambda$, where L represents the characteristic linear size of the scattering surface, and λ is the wavelength of the incident wave. A typical lightning-induced plasma cylinder is kilometers in length and may be meters in diameter, and thus satisfies the condition $L >> \lambda$ in both the $\mathbf{e_r}$ and $\mathbf{e_z}$ directions [Uman, 1969].

Substituting Equations (2) and (3) into the Helmholtz integral (Equation (1)) yields

$$E(P) = \frac{iE_1 e^{ik_2 R_0}}{4\pi R_0} \int\int [R(\mathbf{k_1} - \mathbf{k_2}) \cdot \mathbf{n} - (\mathbf{k_1} + \mathbf{k_2}) \cdot \mathbf{n}] e^{i(\mathbf{k_1} - \mathbf{k_2}) \cdot \mathbf{s}} dA \tag{4}$$

It is convenient to consider the normalized electric field $\hat{E} = E/[iE_1 e^{ik_2 R_0}/4\pi R_0]$. Furthermore, $\mathbf{k_2} = -\mathbf{k_1}$, since monostatic, diagnostic radars were used in the experiments. Equation (4) can thus be rewritten as:

$$\hat{E} = 2R \int\int \mathbf{k} \cdot \mathbf{n} e^{i2\mathbf{k} \cdot \mathbf{s}} dA \tag{5}$$

where $\mathbf{k} = \mathbf{k_1}$; R, the local reflection coefficient at each scattering point, has been aproximated to be constant over the entire surface. This is appropriate for the lightning-induced plasmas, which are almost perfectly conducting, i.e. $|R| \approx 1$ [Williams et al., 1989].

The surface element and normal vector can be written in terms of the density perturbation $\delta s(z)$ as:

$$dA = S d\phi dz \sqrt{1 + (\delta s')^2} \tag{6}$$

$$\mathbf{n} = (-\delta s' \mathbf{e_z} + \mathbf{e_r}) \sqrt{1 + (\delta s')^2}$$

where $\delta s' = \partial(\delta s)/\partial z$. Substituting these terms into Equation (5) yields

$$\hat{E} = 2R \int_0^{\pi} S d\phi \int_{-h/2}^{h/2} dz [-k_z \delta s' + k_r] e^{i2[k_z z + k_r \delta s(z) + k_r S]} \tag{7}$$

where h is the characteristic height of the scattering cylinder.

The mean scattered power can be expressed as $< P >= (1/2) < EE^* > /\eta_0$ where η_0 is the intrinsic impedance of the propagation medium; $\eta_0 = 120\pi \sim 377\ (\Omega)$ for free space. From Equation (7), we may write

$$< \hat{E}\hat{E}^* >= 4\pi^2 S^2 \frac{(k_r^2 + k_z^2)^2}{k_r^2} \int_{-h/2}^{h/2} dz_1 \int_{-h/2}^{h/2} dz_2 e^{i2k_z(z_1 - z_2)} < e^{i2k_r[\delta s(z_1) - \delta s(z_2)]} > \qquad (8)$$

where we have taken $R^2 = 1$.

To proceed further, one must adopt a specific model for the roughness parameter $\delta s(z)$. Plasma irrregularities created by lightning are unlikely to have a periodic or similarly deterministic structure; rather, noise-like, random perturbations are expected. We therefore model the extent of the plasma in the r direction as a random variable $\delta s(z)$, which is completely described by a Gaussian joint probability density function $f[\delta s(z_1), \delta s(z_2)]$ with standard deviation σ, and a normalized autocorrelation function $C(|z_1 - z_2|)$ with characteristic length l and index m:

$$f[\delta s(z_1), \delta s(z_2)] = \frac{1}{2\pi\sigma^2\sqrt{1 - C^2}} \exp(-\frac{\delta s(z_1)^2 - 2C\zeta(z_1)\delta s(z_2) + \delta s(z_2)^2}{2\sigma^2(1 - C^2)}) \qquad (9)$$

$$C(|z_1 - z_2|) = \exp(-|z_1 - z_2|^m / l^m) \qquad (10)$$

Physically, σ and l characterize the height and size of the irregularities of the lightning-induced plasma. Any roughness profile can be approximated by varying the parameters of the joint probability distribution and the autocorrelation function: a large value of σ and a small l imply highly localized peaks with large density variations; by contrast, small σ and large l imply generally low, wide irregularities (see Figure 3). In order to realistically ignore multiple reflections in the model, we have assumed the absence of sharp peaks in the roughness distribution on the surface of the perfectly conducting, lightning-induced plasma; this requirement is satisfied in the regime $l >> \lambda$, $l > \sigma$. Previous authors have concentrated on Gaussian spectra (i.e. $m = 2$ in

Equation (10)) [Isakovich, 1952; Beckmann and Spizzichino, 1963]; studies of transionospheric radio wave propagation have shown, however, that power-law type spectra provide the more realistic model for plasma irregularities [Lee et al., 1989, and references therein]. We therefore take $m = 1$ for the function given in Equation (10).

The definition of the mean in Equation (8) can then be rewritten in terms of the probability density functions as:

$$< e^{2ik_r(\zeta(z_1)-\zeta(z_2))} >= \int_{-\infty}^{\infty} dz_1 \int_{-\infty}^{\infty} dz_2 f(z_1, z_2) e^{2ik_r(z_1-z_2)} \equiv \chi_2(2k_r, -2k_r) \qquad (11)$$

where χ_2 is the two-dimensional characteristic function of the joint probability distribution $f(z_1, z_2)$. Similarly, the one-dimensional characteristic function is defined as

$$\chi(2k_r) \equiv< e^{2ik_r z} >= \int_{-\infty}^{\infty} f(z) e^{i2k_r z} dz \qquad (12)$$

where $f(z) = (\sqrt{2\pi}\sigma)^{-1} \exp(-z^2/2\sigma^2)$. It is useful to first calculate the variance, $\mathrm{d}(\hat{E}) = < \hat{E}\hat{E}^* > - < \hat{E} >< \hat{E} >^*$, given by

$$d(\hat{E}) = 4\pi^2 S^2 \frac{(k_r^2 + k_z^2)^2}{k_r^2} \int_{-h/2}^{h/2} dz_1 \int_{-h/2}^{h/2} dz_2 e^{i2k_z(z_1-z_2)} [\chi_2(2k_r, -2k_r) - \chi(2k_r)\chi^*(2k_r)] \qquad (13)$$

For a Gaussian joint probability distribution function, $\chi(2k_r) = exp(-2k_r^2\sigma^2)$ and $\chi_2(2k_r, -2k_r) = \exp[-4k_r^2\sigma^2(1 - C)]$; thus Equation (13) becomes

$$d(\hat{E}) = 4\pi^2 S^2 \frac{(k_r^2 + k_z^2)^2}{k_r^2} \int_{-h/2}^{h/2} dz_1 \int_{-h/2}^{h/2} dz_2 e^{i2k_z(z_1-z_2)} [e^{-4k_r^2\sigma^2(1-C)} - e^{-4k_r^2\sigma^2}] \qquad (14)$$

The integrand vanishes when $C = 0$, or when $|z_1 - z_2|$ is large; thus we may appoximate $C = \exp(-|z_1 - z_2|)/l \approx 1 - |z_1 - z_2|/l$ and replace the integration limits for z_2 by $z_1 \pm l \geq z_2$, where l is the maximum range of $|z_1 - z_2|$ for which the first order approximation to the exponential

is valid. This is a good approximation insofar as the integrand in Equation (14) is localized within $\pm l$; it can be seen that this is the case for a very rough surface, i.e.: $4k_r^2\sigma^2 >> 1$, which is the relevant regime for the lightning backscatter experiments considered here. Integrating the expression in Equation (14) and neglecting terms on the order of $e^{-4k_r^2\sigma^2}$ yields the following final result:

$$< P > \propto < \hat{E}\hat{E}^* > \approx 32h\pi^2 S^2 \frac{(k_r^2 + k_z^2)^2}{k_r^2} \left[\frac{k_r^2\sigma^2/l}{16k_r^4\sigma^4/l^2 + 4k_z^2}\right] \tag{15}$$

The term $(k_r^2 + k_z^2) = k^2 - k_\phi^2$ indicates that $< P >= 0$ for $k = k_\phi$; i.e. the backscattered power is zero for grazing incidence of the radio waves on the plasma cylinders, as expected.

The result may be applied only where the approximation used in evaluating the integral in Equation (14) is justified; this is the case for $4k_r^2\sigma^2 >> 1$. Multiple reflections from the scattering surface may be ignored only insofar as the density irregularities are smooth; this condition is met when $l >> \lambda$. Furthermore, if $k_z^2 >> 4k_r^4\sigma^4/l^2$, it can be shown that

$$< P > \approx \frac{h}{2}\frac{S^2}{\pi^2}\frac{\sigma^2}{l}\frac{(k_r^2 + k_z^2)^2}{k_z^2} \propto 1/\lambda^2 \tag{16}$$

which is in agreement with the experimental results described in Section 2.

4 Reflectivity of Single Radio Beam Produced Plasma Disks

4.1 Diagnostics with a Monostatic Radar

The success of the rough surface scattering model in explaining the radio reflectivity of lightning-induced plasma channels suggests that it may be usefully employed to predict the behavior of a

radio wave induced plasma patch. In this section the analysis outlined in Section 3 is applied to the pancake or disk-shaped plasmas produced by a single radio beam.

The plasma patch is modeled as a disk of radius S and height h, centered at the origin of a cylindrical coordinate system. Vectors from the origin to the the bottom surface of the disk are given by $\mathbf{s} = r\mathbf{e_r} + [\delta z(r,\phi) - h/2]\mathbf{e_z}$, where $\delta z(r,\phi)$ is the random variable describing the height fluctuations of the plasma, characterized by the Gaussian joint probability distribution given in Equation (9) (See Figure 4). It is reasonable to assume that the autocorrelation function of δs is a function of radius only; i.e. $C(|r_1 - r_2|) = \exp(-|r_1 - r_2|^m/l^m)$. Thus the surface density distribution of the plasma patches can be taken to be azimuthally symmetric, or $\delta z(r,\phi) = \delta z(r)$. Under these conditions, one may write, in analogy to Equations (6),

$$\hat{\mathbf{n}} = (\mathbf{e_z} - \delta z'\mathbf{e_r})/\sqrt{1 + (\delta z')^2} \tag{17}$$

$$dA = \sqrt{1 + (\delta z')^2} r dr d\phi \tag{18}$$

where $\delta z' = \partial(\delta z)/\partial r$. Substituting Equations (17) and (18) into the Helmholtz integral for a monostatic radar (Equation (5)) gives the following expression for the detected electric field:

$$\hat{E} = 2Re^{-ik_z h} \int_0^{2\pi} d\phi \int_0^S dr[k_z - k_r \delta z'] e^{2i[k_r r + k_z \delta z(r)]} \tag{19}$$

Following the method of analysis described in Section 3, the standard deviation of the normalized electric field is found to be:

$$d(\hat{E}) = 16\pi^2 R^2 \int_0^S dr_2 \int_{r_2 - l}^{r_2 + l} dr_1 [A r_1 r_2 + B(r_2 - r_1) + C] e^{2ik_r(r_1 - r_2)} [e^{-4k_z^2\sigma^2|r_1 - r_2|} - e^{-4k_z^2\sigma^2}] \tag{20}$$

where $A = k_z^2 + 2k_r^2 + k_r^4/k_z^2 = k^4/k_z^2$, $B = (k_r/2i)[1 + k_r^2/k_z^2]$, and $C = k_r^2/(4k_z^4)$. For $4k_z^2\sigma^2 >> 1$, the integrand is negligible for $|r_1 - r_2| > 1$. Thus we may make the transformation $\rho = r_1 - r_2$ and estimate the integral in Equation (20) by

$$d(\hat{E}) = \int_0^S dr_2 \int_{-l}^{l} d\rho [A(r_2^2 + \rho) + B\rho + C] e^{i2k_r\rho} [e^{-4k_z^2\sigma^2|\rho|/l} - e^{-4k_z^2\sigma^2}] \tag{21}$$

$$\approx \int_0^S dr_2 \int_{-l}^{l} d\rho [A(r_2^2) + B\rho + C] e^{i2k_r\rho} [e^{-4k_z^2\sigma^2|\rho|/l} - e^{-4k_z^2\sigma^2}]$$

Evaluating the integral in Equation (21) gives the following expression for the backscattered power:

$$< P > \propto < \hat{E}\hat{E}^{*} > \approx 16\pi^{2}[\frac{2S^{3}k^{4}\sigma^{2}/l}{12k_{z}^{4}\sigma^{4}/l^{2}+3k_{r}^{2}} + \frac{S^{2}k_{r}^{2}}{4k_{z}^{2}} + (Sk_{r}/8)[1+k_{r}^{2}/k_{z}^{2}]\frac{k_{r}+2k_{z}^{2}\sigma^{2}/l}{(4k_{z}^{4}\sigma^{4}/l^{2}+k_{r}^{2})^{2}}] \quad (22)$$

where we have taken $R^2 = 1$, and where a power-law type of irregularity spectrum [i.e., $m = 1$ in the autocorrelation function given in Equation (10)] has been assumed. Terms on the order of $\exp(-4k_z^2\sigma^2)$ have been neglected in Equation (22). We consider the case analogous to the lightning-induced plasmas, i.e. the surface is large ($S >> \lambda$), with significant, smooth surface fluctuations ($l/\sigma > 1$, $l >> \lambda$, $4k_z^2\sigma^2 >> 1$). Under these conditions, the first term in Equation (22) is dominant, and thus the backscattered power may be expressed as:

$$< P > \approx \frac{S^{3}}{R_{0}^{2}}\frac{2k^{4}\sigma^{2}/l}{12k_{z}^{4}\sigma^{4}/l^{2}+3k_{r}^{2}} \quad (23)$$

This result is basically the same as that found for the lightning induced plasmas, given by Equation (15).

If a Gaussian autocorrelation function is used (i.e. $m = 2$ in Equation (10)), the backscattered power is given by

$$< P > \approx \sqrt{\pi}(l/2\sigma)(k^{4}/k_{z}^{3})(S^{3}/3R_{0}^{2})\exp(-k_{r}^{2}l^{2}/4k_{z}^{2}\sigma^{2}) \quad (24)$$

While convincing evidence shows that the density irregularities of the lightning-induced plasmas have a power-law type of spectrum, it is unclear what type of irregularity spectrum may be produced by a single radio beam induced plasma patch. In the case of a power-law spectrum, the radio reflectivity of the pancake plasmas is expected to behave analogously to the lightning-induced plasma; by contrast, if the irregularities are more properly described by a Gaussian spectrum, the radio reflectivity may be wavelength dependent.

4.2 Radio Communication/Space Surveillance with a Bistatic Radar

In radio communication or space surveillance applications of the artificially produced plasmas, bistatic radars will be employed. In this geometry, the incident wave vector ($\mathbf{k_1}$) and the detected, reflected wave vector ($\mathbf{k_2}$) are described by $\mathbf{k_1} = k_r\mathbf{e_r} + k_z\mathbf{e_z}$; $\mathbf{k_2} = k_r\mathbf{e_r} - k_z\mathbf{e_z}$. The $\mathbf{k_2}$ direction is the specular direction of reflection.

The Helmholtz integral (Equation (5)) thus reduces to

$$\hat{E} = 2\int\int_A [Rk_z + k_r\zeta_r']e^{i2k_z[\zeta(r)-h/2]}rdrd\phi \tag{25}$$

which may be used to solve for the power reflected in the $\mathbf{k_2}$ direction:

$$d(\hat{E}) = \int_0^S dr_2 \int_{r_2-l}^{r_2+l} dr_1[k_z^2 r_1 r_2 - ik_r/2(r_1 - r_2) + k_r^2/(4k_z^2)][e^{-4k_z^2\sigma^2|r_1-r_2|/l} - e^{-4k_z^2\sigma^2}] \tag{26}$$

$$< P > \propto d(\hat{E}) + < \hat{E} > \hat{E} >^* = \tag{27}$$

$$16\pi^2\Big[\frac{S^3 l}{6\sigma^2} + \frac{k_r^2 Sl}{8k_z^4\sigma^2} - 2le^{-4k_z^2\sigma^2}[k_z^2 S^3/3 + k_r^2 S/(4k_z^2)] + S^2k_r^2/(4k_z^2)\Big]$$

In the derivation of Equation (27), a power-law type of irregularity spectrum [i.e. $m = 1$ in Equation (10)] has been assumed. Under the conditions assumed in Section 3, the first term dominates, and the power may be expressed as:

$$< P > \propto (1/6)\frac{S^2}{R_0^2}(S/\sigma)(l/\sigma) \tag{28}$$

This result is independent of both the wavelength and the angle of incidence. Thus the pancake plasmas do not preferentially scatter any one wavelength into the specular direction, if the plasma irregularities have power-law spectra. Equation (28) also indicates that smoother surfaces (i.e., S/l, l/σ large) scatter more power into the specular direction, as expected.

If a Gaussian autocorrelation function is assumed, the reflected power is found to be

$$< P > \approx (1/6)\sqrt{\pi} k_z (S^3/R_0^2) l/\sigma \tag{29}$$

indicating that if the surface density irregularities are more properly described by a Gaussian spectrum, the power reflected into the specular direction will be larger for longer wavelengths at any given angle of incidence. As mentioned earlier, it is unclear whether the radio wave produced plasma patch has a power-law or Gaussian type of plasma irregularity spectrum. These theoretical results can thus serve as a means of diagnosing the structure of the artificial plasma disk.

5 Conclusions

The wavelength dependence of the backscattered power from lightning-induced plasmas has been studied in experiments conducted with the MIT S-band, C-band, and the Millstone UHF radars. The average reflected power was observed to decrease with the wavelength as $1/\lambda^2$. This behavior can be successfully explained by the scattering of electromagnetic waves from the small-scale density irregularities of the lightning-induced, perfectly conducting plasma channels in the atmosphere. These density irregularities are reasonably assumed to have a power-law rather than a Gaussian spectrum. A region of validity for the predicted $1/\lambda^2$ relation is believed to exist in the experiments, which depends on the expected size of the density irregularities (σ/l), and the angle of incidence of the radio waves on the plasma channels.

Similar results are derived in the case of monostatic reflection of radio waves from an artificially produced plasma pancake. In bistatic radio communication/space surveillance applications,

the reflected power is expected to have no wavelength dependence, if the plasma irregularities have a power-law spectrum. By contrast, if the surface density irregularities are characterized by a Gaussian spectrum, the reflected power is inversely proportional to the incident radio wavelength. Since radio communications applications of artificial plasma patches intend primarily to extend ionospheric reflection to higher frequencies, this should not seriously limit the efficiency of the proposed schemes. Thus it is expected that radio wave induced plasma patches may be efficiently employed over a broad range of frequencies to extend radio communication paths beyond their present capabilities

Acknowledgments. This work is supported by NSF Grant No. ATM-9016235 and AFOSR Grant No. F49620-92-J-0103 and Grant No. AFOSR-92-0001.

6 References

- Beckmann, P., and A. Spizzichino, *The Scattering of Electromagnetic Waves from Rough Surfaces,* Pergamon Press, New York, 1963.

- Dalkir, Y.R., M.C. Lee, E.R. Williams, Radio Reflectivity of lightning-induced plasmas, to be submitted to JGR for publication.

- Gurevich, A.V., An ionized layer in a gas (in the atmosphere), *Sov. Phys. Usp., 23,* 862, 1980.

- Isakovich, M. A., The scattering of waves from a statistically rough surface (in Russian), *Zhurn. Eksp. Teor. Fiz., 23,* 305, 1952.

- Kuo, S.P., Y.S. Zhang, M.C. Lee, P.A. Kossey, and R.J. Barker, An experimental study of OTH radar using Bragg reflection from artificially ionzied layers of a gas, to appear in Radio Sci., 1992.

- Lee, M.C., D. Thurairatnam, and E.R. Williams, Radio wave scattering from artificial plasma layers, paper presented at URSI/National Radio Science Meeting, Boulder, CO, Jan., 1988.

- Lee, M.C., S. V. Nghiem, and C. Yoo, Effects of irregularity anisotropy on Faraday polarization fluctuations, *J. Geophys. Res., 94,* 15,421, 1989.

- Short, R. et al., Physics study in artificial ionospheric mirror (AIM) related phenomena, *Technical Final Report,* GL-TR-90-0038.

- Uman, M. A., *Lightning,* McGraw-Hill, New York, 1969.

- Williams, E.R., S.G. Geotis, and A.B. Bhattacharya, A radar study of the plasma and geometry of lightning, *J. Atmos. Sci., 46,* 1173, 1989.

7 Figure Captions

Fig. 1. Summary of experimental results. The average volume reflectivity at $\lambda = 5.4$, 11 and 68 cm is plotted. The numbers in parentheses indicate the number of data points collected. The wavelength dependence predicted by the theory of long thin conductors, and underdense plasma channels is also indicated on the figure. Neither existing model fits the data of the present study, which exhibit a clear $1/\lambda^2$ dependence.

Fig. 2. Schematic representation of overall scattering geometry. The transmitter is located a few kilometers from the lightning activity. Radio signals with wave vector $\mathbf{k}$ are incident on the plasma surface at an angle θ to the horizontal. The z axis is taken to along the axis of symmetry of the plasma channel, which is approximately perpendicular to the ground. The position vector s extends from the origin of the coordinate system to the surface of the lightning-induced plasma; $\mathbf{n}$ is the local normal vector to the surface. h is the vertical extent of the plasma, which is estimated to be on the order of kilometers.

Fig. 3. Section of lightning-induced plasma, showing smooth surface irregularities with characteristic parameters σ and l (figure not drawn to scale). The geometry illustrates the relation $k_2 R' = k_2 R_0 - \mathbf{k_2} \cdot \mathbf{s}$ used after Equation (1).

Fig. 4. Geometry of radio wave scattering from plasma disks of radius S and height h. The heater array "paints" the plasma patch through air breakdown in the beam cross-section. The transmitted wave is incident on the plasma at the origin of a cylindrical coordinate system. In the diagnostic geometry, $\mathbf{k_{backscatter}} = -\mathbf{k_{transmitted}}$. In radio communication applications, the reflected wave is in the $\mathbf{k_{specular}}$ direction. Note that the scattering surface is not flat, but irregular in the $\mathbf{e_z}$ direction (not pictured).

Figure 4

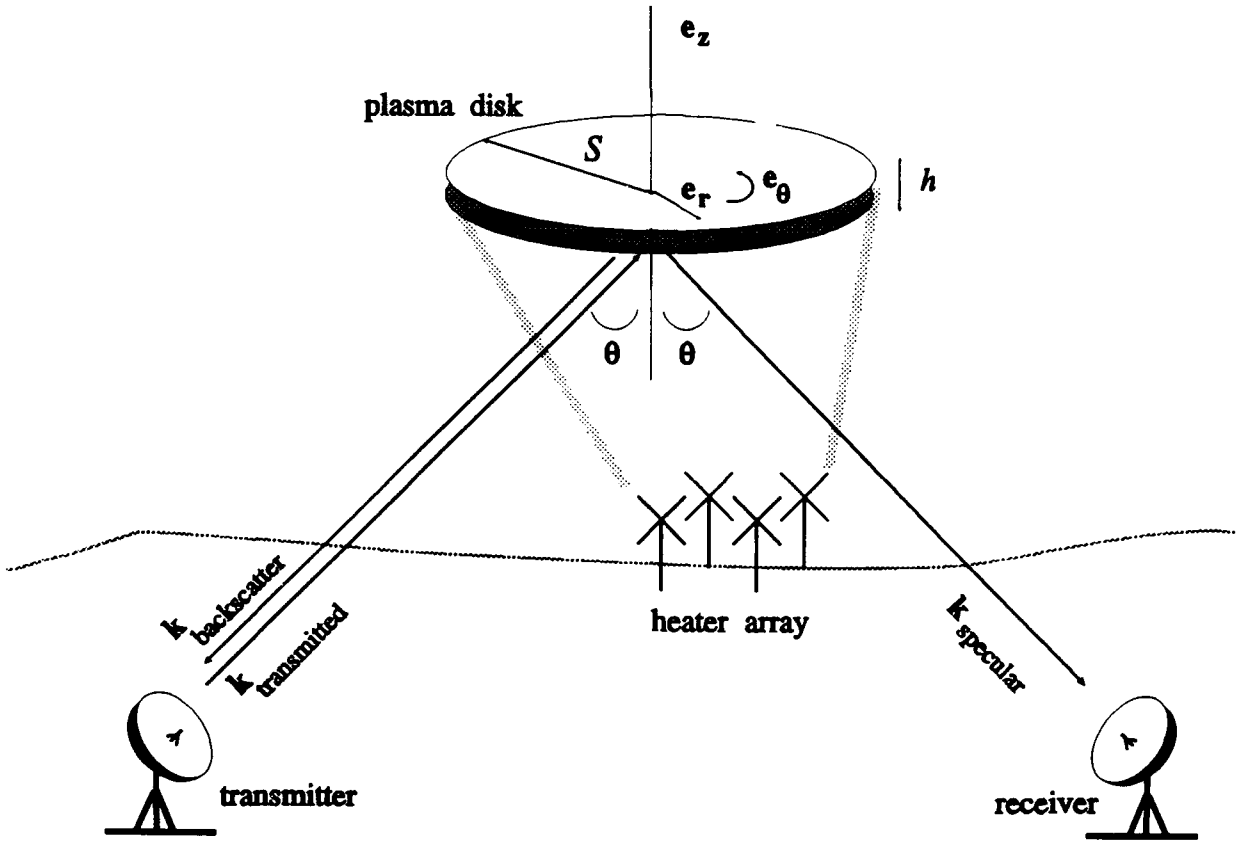
e_z
plasma disk
S
e_r
e_θ
h
θ
θ
$k_{backscatter}$
$k_{transmitted}$
heater array
$k_{specular}$
transmitter
receiver